Department of Electrical Engineering and Automation

Photovoltaic Hosting Capacity of Distribution Networks

Verner Püvi

Aalto University

DOCTORAL THESES

Aalto University publication series
DOCTORAL THESES 129/2024

Photovoltaic Hosting Capacity of Distribution Networks

Verner Püvi

A doctoral thesis completed for the degree of Doctor of Science (Technology) to be defended, with the permission of the Aalto University School of Electrical Engineering, at a public examination held at the lecture hall TU1 of the school on the 1st of July 2024 at 12:00.

Aalto University
School of Electrical Engineering
Department of Electrical Engineering and Automation
Power Systems and High Voltage Engineering

Supervising professor
Professor Matti Lehtonen, Aalto University, Finland

Thesis advisor
Professor Matti Lehtonen, Aalto University, Finland

Preliminary examiners
Doctor Victor Astapov, Tallinn University of Technology, Estonia
Associate Professor Jukka Lassila, Lappeenranta-Lahti University of Technology, Finland

Opponent
Professor Mikko Kolehmainen, University of Eastern Finland, Finland

Aalto University publication series
DOCTORAL THESES 129/2024

ISBN 978-952-64-1884-1 (printed)
ISBN 978-952-64-1885-8 (pdf)
ISSN 1799-4934 (printed)
ISSN 1799-4942 (pdf)
http://urn.fi/URN:ISBN:978-952-64-1885-8

Unigrafia Oy
Helsinki 2024

Finland

NORDIC SWAN ECOLABEL
Printed matter
4041-0619

Author
Verner Püvi

Name of the doctoral thesis
Photovoltaic Hosting Capacity of Distribution Networks

Publisher School of Electrical Engineering

Unit Department of Electrical Engineering and Automation

Series Aalto University publication series DOCTORAL THESES 129/2024

Field of research Power Systems and High Voltage Engineering

Manuscript submitted 22 March 2024 **Date of the defence** 1 July 2024

Permission for public defence granted (date) 26 April 2024 **Language** English

☐ **Monograph** ☒ **Article thesis** ☐ **Essay thesis**

Abstract

Due to an increasing share of renewable energy sources and widespread adoption of distributed photovoltaics (PV), the ability of the distribution networks to reliably interconnect new PV installations without hindering the power system's operation gained a lot of interest in the recent decade. Political support and falling prices of the photovoltaics make the panels available for as small as single household installations and some of the network operators have already reported the power quality issues caused by the PVs.

To address this issue, this thesis investigates the PV hosting capacity (HC) of low-voltage distribution networks. The thesis is split into two main contributions centered around the power quality limitations of the HC and network structure influence on the HC. The thesis starts with a review of the HC definitions, its most common limiting factors, and reports on the results of a measurement campaign of low-voltage substations.

In the first part, a Monte Carlo-based HC evaluation methodology is presented, which is used for the PV-only and energy storage-augmented scenarios. Alongside the single-phase PV installations, a voltage unbalance (VU) mitigation methodology is presented. Despite the VU being a very strict limit, it can be mitigated by relatively low power injections. Moreover, a comparison of PV curtailment and network reinforcement is presented to find the break-even points of the costs of the two. The second part of the thesis presents the distribution network's structure impact on the hosting capacity. A fixed set of customers is simulated with multiple feeding substations and a varying number of PV plants. The slime mold algorithm was proposed to be employed for generating numerous network topologies and its advantages over other algorithms were shown. The results revealed that around one-third of the customers can have PV installations until the HC is depleted. Voltage control can increase the HC, however remains the risk of possible need to change residential PV policies to sustain the current pace of PV installations. Finally, the thesis explores the practical side of the HC and analyzes the accuracy of distribution network state estimation. A PV safety margin is proposed, that represents an equivalent PV power that has to be curtailed in order to keep the estimated values below the actual values of the states.

Keywords distribution networks, hosting capacity, network structure, optimization, photovoltaics, power quality, state estimation

ISBN (printed) 978-952-64-1884-1 **ISBN (pdf)** 978-952-64-1885-8

ISSN (printed) 1799-4934 **ISSN (pdf)** 1799-4942

Location of publisher Helsinki **Location of printing** Helsinki **Year** 2024

Pages 245 **urn** http://urn.fi/URN:ISBN:978-952-64-1885-8

Abstract

Due to an increasing share of renewable energy sources and widespread adoption of distributed photovoltaics (PV), the ability of the distribution networks to reliably interconnect new PV installations without hindering the power system's operation gained a lot of interest in the recent decade. Political support and falling prices of the photovoltaics make the panels available for as small as single household installations and some of the network operators have already reported the power quality issues caused by the PVs.

To address this issue, this thesis investigates the PV hosting capacity (HC) of low-voltage distribution networks. The thesis is split into two main contributions centered around the power quality limitations of the HC and network structure influence on the HC. The thesis starts with a review of the HC definitions, its most common limiting factors, and reports on the results of a measurement campaign of low-voltage substations.

In the first part, a Monte Carlo-based HC evaluation methodology is presented, which is used for the PV-only and energy storage-augmented scenarios. Alongside the single-phase PV installations, a voltage unbalance (VU) mitigation methodology is presented. Despite the VU being a very strict limit, it can be mitigated by relatively low power injections. Moreover, a comparison of PV curtailment and network reinforcement is presented to find the break-even points of the costs of the two. The second part of the thesis presents the distribution network's structure impact on the hosting capacity. A fixed set of customers is simulated with multiple feeding substations and a varying number of PV plants. The slime mold algorithm was proposed to be employed for generating numerous network topologies and its advantages over other algorithms were shown. The results revealed that around one-third of the customers can have PV installations until the HC is depleted. Voltage control can increase the HC, however remains the risk of possible need to change residential PV policies to sustain the current pace of PV installations. Finally, the thesis explores the practical side of the HC and analyzes the accuracy of distribution network state estimation. A PV safety margin is proposed, that represents an equivalent PV power that has to be curtailed in order to keep the estimated values below the actual values of the states.

Preface

This dissertation summarizes the key findings of my work as a doctoral candidate at the Department of Electrical Engineering and Automation, Aalto University, Finland between 2018 and 2024. This work was supported by the Finnish Public Funding Agency for Research, Business Finland, through projects Finnish Solar Revolution (FSR), SolarX, Smart Grid 2.0, and IFORGE.

I would like to express my deep gratitude to Prof. Matti Lehtonen for providing me with the invaluable opportunity to pursue my PhD studies. Your mentorship, constructive feedback, and friendly support have been instrumental in shaping this journey. Your positive attitude had a confidence-inspiring impact on me. Moreover, I would also like to acknowledge the pre-examiners of this thesis, Dr. Victor Astapov From Tallinn University of Technology and Assoc. Prof. Jukka Lassila from Lappeenranta-Lahti University of Technology.

I extend my sincere thanks to Dr. Toni Tukia and Dr. Simo Uimonen for being such insightful examples, your experiences helped me decide to pursue my own PhD. I would also like to express my gratitude to the entire group of colleagues including Dr. John Millar, Dr. Arslan Ahmad Bashir, Dr. Mehdi Tavakkoli, David Sevsek, Asst. Prof. Mahdi Pourakbari Kasmaei, Fatima Samar, Xinyi Hu, Amin Moghimy Fam, Mahyar Tofighi Milani, Ilkka Jokinen, Dr. Ammar Arshad, and Dr. Jussi Ekström, also my sauna team, for engaging in enlightening discussions, sharing knowledge, and contributing to a collaborative and stimulating research environment. Thanks to the rest of the people in the office for building a friendly working atmosphere.

Big thanks to my peers during exchange studies at the National Institute of Informatics (NII), including Tahitoa Arbelot, David Sarda, Dr. Simon Luo, and Dr. Colin Leverger for enriching experience and diverse perspectives. Special gratitude to Prof. Ken Hayami for making the exchange studies in Tokyo possible and giving me the opportunity to collaborate in a multidisciplinary team. This venture turned out to be truly life-changing.

I wish to show appreciation to Assoc. Prof. Lauri Kütt from Tallinn University of Technology, Dr. Eero Saarijärvi, Caruna Networks Oy, and Helen Sähköverkko Oy for their valuable contributions and collaborative efforts.

I am deeply indebted to my family – my mother, sister, father, and other family members – for their firm support, encouragement, and understanding throughout this academic endeavor. Their love has been a constant source of strength for me.

A special acknowledgment goes to my wife Mihoko-san for her remarkable patience, support, and understanding during this challenging period. Your encouragement has been a driving force, and I am truly grateful. Ganbatte!

Espoo, February 6, 2024,

Verner Püvi

Contents

Preface **3**

Contents **5**

List of Publications **7**

Author's Contribution **9**

List of Figures **11**

List of Tables **13**

Abbreviations **15**

Symbols **17**

1. Introduction **21**
1.1 Background and Motivation 21
1.2 Objective and Tasks 22
1.3 Scientific Contribution 24
1.3.1 Power Quality 24
1.3.2 Network Structure 25
1.3.3 Practical Implications 25
1.4 Dissertation Outline 26

2. Preliminary Basics **27**
2.1 Photovoltaic Hosting Capacity 27
2.1.1 Hosting Capacity Definitions 27
2.1.2 Photovoltaic Penetration Limiting Factors 29
2.2 Test Networks 31
2.3 Power Quality Survey 32
2.4 Photovoltaic Generation 34

3. Power Quality **35**
3.1 Literature Review 35

3.2 Hosting Capacity Analysis 38
3.2.1 Hosting Capacity Evaluation Methodology 39
3.2.2 Case Studies and Simulation Results 42
3.3 Voltage Unbalance Mitigation 45
3.3.1 Proposed Voltage Unbalance Optimization Model . 45
3.3.2 Case Studies and Simulation Results 50
3.4 Chapter Conclusions 52

4. Network Structure **55**
4.1 Literature Review 55
4.2 Topology Generation 57
4.2.1 The Slime Mold Algorithm 57
4.2.2 Comparative Simulation and Results 62
4.3 Optimal Network Size 65
4.3.1 Proposed Simulation Model 66
4.3.2 Case Studies and Simulation Results 68
4.4 Chapter Conclusions 72

5. Practical Implications **75**
5.1 Literature Review 75
5.2 State Estimation and the PV Safety Margin 76
5.3 Case Study and Simulation Results 79
5.4 Chapter Conclusions 83

6. Discussions **85**

References **89**

Publications **99**

List of Publications

This thesis consists of an overview and of the following publications which are referred to in the text by their Roman numerals.

I Fatima, S., **Püvi, V.**, & Lehtonen, M. Review on the PV Hosting Capacity in Distribution Networks. *Energies*, Volume 13, issue 18, article number 19, September 2020.

II **Püvi, V.**, Tukia, T., Lehtonen, M., & Kütt, L. Survey of a Power Quality Measurement Campaign in Low-Voltage Grids. In *2019 Electric Power Quality and Supply Reliability Conference (PQ) & 2019 Symposium on Electrical Engineering and Mechatronics (SEEM)*, Kärdla, Estonia, 1-7, August 2019.

III Arshad, A., **Püvi, V.**, & Lehtonen, M. Monte Carlo-Based Comprehensive Assessment of PV Hosting Capacity and Energy Storage Impact in Realistic Finnish Low-Voltage Networks. *Energies*, Volume 11, issue 6, article number 1467, June 2018.

IV Fatima, S., **Püvi, V.**, Pourakbari-Kasmaei, M., & Lehtonen, M. Photovoltaic Hosting Capacity Improvement Based on the Economic Comparison Between Curtailment and Network Upgrade. *IET Generation, Transmission & Distribution*, Volume 17, issue 17, pages 3848–3860, July 2023.

V **Püvi, V.**, & Lehtonen, M. Convex Model for Estimation of Single-Phase Photovoltaic Impact on Existing Voltage Unbalance in Distribution Networks. *Applied Sciences*, Volume 10, issue 24, article number 8884, December 2020.

VI **Püvi, V.**, Millar, R. J., Saarijärvi, E., Hayami, K., Arbelot, T., & Lehtonen, M. Slime Mold Inspired Distribution Network Initial Solution. *Energies*, Volume 13, issue 23, article number 6278, November 2020.

VII **Püvi, V.**, & Lehtonen, M. Evaluating Distribution Network Optimal Structure with respect to Solar Hosting Capacity. *Electric Power Systems Research*, Volume 216, article number 109019, March 2022.

VIII **Püvi, V.**, & Lehtonen, M. Photovoltaic Hosting Capacity Margin due to State Estimation Error. Submitted to *International Review of Electrical Engineering*, January 2024.

Author's Contribution

In five of the publications (Publications II and V-VIII), the author of the thesis has the highest contribution. The author was responsible for developing ideas and concepts, conducting the simulations, analyzing the results, and finally writing the research papers. Contributions of the co-authors and the rest of the publications (Publications I, III, and IV) are indicated in the following.

Publication I: "Review on the PV Hosting Capacity in Distribution Networks"

Fatima, S. made the largest contribution by doing the literature survey and writing the article. Püvi, V. contributed to the methodology of the literature analysis and reviewed the draft. Lehtonen, M. commented on the draft and supervised the work.

Publication II: "Survey of a Power Quality Measurement Campaign in Low-Voltage Grids"

Tukia, T. contributed to the measurement set-ups and validated the results. Kütt, L. contributed through his detailed comments and feedback on results. Lehtonen, M. supervised the work.

Publication III: "Monte Carlo-Based Comprehensive Assessment of PV Hosting Capacity and Energy Storage Impact in Realistic Finnish Low-Voltage Networks"

Arshad, A. made the largest contribution by conducting the simulations and writing the main body of the article. Püvi, V. contributed by introducing the battery model, processing the load voltage unbalance data, and reviewing the draft. Lehtonen, M. supervised the work.

Publication IV: "Photovoltaic Hosting Capacity Improvement Based on the Economic Comparison Between Curtailment and Network Upgrade"

Fatima, S. made the largest contribution by conducting the simulations and writing the main body of the article. Püvi, V. contributed with methodology and reviewing the draft. Lehtonen, M. supervised the work.

Publication V: "Convex Model for Estimation of Single-Phase Photovoltaic Impact on Existing Voltage Unbalance in Distribution Networks"

Lehtonen, M. supervised the work.

Publication VI: "Slime Mold Inspired Distribution Network Initial Solution"

Millar, R. J., Saarijärvi, E., and Arbelot, T. contributed by suggesting to investigate the slime mold algorithm, commented on the mathematical formulation, and reviewed the test results of the algorithm. Hayami, K. and Lehtonen, M. supervised the work.

Publication VII: "Evaluating Distribution Network Optimal Structure with respect to Solar Hosting Capacity"

Lehtonen, M. participated in developing the methodology and supervised the work.

Publication VIII: "Photovoltaic Hosting Capacity Margin due to State Estimation Error"

Lehtonen, M. participated in developing the methodology and supervised the work.

List of Figures

2.1 Utilized hosting capacity definitions in the reviewed literature. 28
2.2 Percentages of the limiting factors in the literature showing voltage violations as the most pronounced limiting constraint. 29
2.3 Networks modeled in the current thesis for (a) rural, (b) suburban, and (c) urban regions. Numbers denote node indices. 31
2.4 Probability and cumulative distribution functions of the negative sequence voltage unbalance collected at all the measurement sites. 32
2.5 The ratio of mean and maximum current of each feeder supplying households (hh) and one apartment building (ap). Three data aggregation time resolutions are presented: 10-second, 10-minute, and 1-hour. 33
2.6 Curves of clear-sky PV output and a case of an actual PV output. 34

3.1 Flowchart of the hosting capacity calculation for a network with PV, BESS, and background VU. 39
3.2 The window of worst case hours over one year capturing critical hours of the highest PV generation and (a) lowest load, and (b) highest BESS charging power. 40
3.3 Photovoltaic curtailment realized in the current analysis by decreasing PV peak power. 42
3.4 The cost comparison of the network reinforcement and PV curtailment for the three regions (a) rural, (b) suburban, and (c) urban. 44
3.5 Flowchart of the Monte Carlo simulation assessing VU mitigation. 49
3.6 Maximum PV injection at fixed phases. 50

3.7 Voltage unbalance attenuation at strategy 3 (a) and corresponding PV injection (b). 51
3.8 Maximum PV injection at optimal phase selection. 51
3.9 Voltage unbalance attenuation with optimal phase (a) and corresponding PV injection (b) at the lowest and highest background VU 52

4.1 Flowchart of the slime mold algorithm. 60
4.2 Topology types for the same set of nodes (a) MST, (b) Slime Mold solution, and (c) Star topology. 61
4.3 Cost function values of the Slime Mold Algorithm solutions. 61
4.4 Average cost of rural networks (a), and the cost and the computation time of each network (b). 64
4.5 Average cost of suburban networks (a), and the cost and the computation time of each network (b). 64
4.6 Average cost of urban networks (a), and the cost and the computation time of each network (b). 65
4.7 Flowchart of the proposed framework 67
4.8 The topology of MV network with 75 LV substations. A callout of underlying LV networks of the suburb region. . . 69
4.9 Cost and the number of violations dependency on the number of substations in suburb region for the base case 70
4.10 Voltage control in comparison to optimal, smaller (TF-) or larger (TF+) number of substation. 71
4.11 Hosting capacity (HC) as average PV injected power per customer. 71

5.1 Average and 5-95th percentile values of the estimation error of rural network in balanced condition. The base case has only pseudo-measurements and voltage real-time measurement at the feeding transformer; setup B1 implies an additional current magnitude real-time meter at the transformer. 80
5.2 PV margin caused by voltage rise at different measurement setups and frequencies in the (a) rural and (b) urban networks. 81
5.3 Comparison of the phase a voltage of the base case with the RPV (A1) and real-time current meter setup (B1) in the rural network. 82

List of Tables

2.1 Hosting Capacity definitions based on the literature review. 28
2.2 Transformer rating and cable parameters of the test networks. 31
2.3 Transformer parameters (0.4/20 kV) 32
2.4 Household heating types are listed in likelihoods for each region: storage heating, non-electric heating, and direct electric heating. 32

3.1 Hosting capacity (HC) of three- and single-phase PV cases. Also, a mixed PV case is shown with the ratios of single-phase PVs, which causes the unbalance violations. Hosting capacity as % of transformer rating. 43
3.2 Hosting capacity (HC) of the mixed PV case with BESS. Three BESS strategies are shown: BESS connected to random phase, same phase with PV, and additionally introduced background VU. Hosting capacity as % of transformer rating. 43

4.1 Network cost parameters for the Slime Mold Algorithm analysis 58
4.2 Network parameters for the slime mold algorithm tests. . 62
4.3 MV cable parameters 68
4.4 Maximum feasible share of customers (%) with PV plants if average PV plant sizes are 6 and 9.25 kWp 72

5.1 Measurement variances for pseudo-measurements, reference PV (RPV), and real-time voltage and current measurements 78

Abbreviations

BESS Battery Energy Storage System

DER Distributed Energy Resources

DERMS DER Management System

DSO Distribution System Operator

HC Hosting Capacity

LV Low-Voltage

MAPE Mean Absolute Percentage Error

MIQP Mixed-Integer Quadratic Programming

MST Minimum Spanning Tree

MV Medium-Voltage

NPA Network Planning Algorithm

NWA Non-Wire Alternative

OLTC On-Load Tap Changer

OPF Optimal Power Flow

PV Photovoltaic

QP Quadratic Programming

RPC Reactive Power Control

RPV Reference Photovoltaic

SE State Estimation

SM Smart Meter

WLS Weighted Least Squares

Symbols

In this thesis, underlined letters such as $\underline{V_a}$ are used to denote vectors.

a Phasor rotation operator ($1 \cdot \angle 120°$)

c^c Cost of cables

c^{CB} Total cost of cables

c^{curt} Cost of curtailed energy

c^e Cost of energy losses

c^{inv} Investment cost

c^{loss} Loss costs

c^{maint} Cost of an OLTC transformer maintenance

$c^{MV,CB}$ Medium voltage cable investment cost

c^{OLTC} Total cost of OLTC maintenance

c^t Cost of a single transformer

c^{TF} Total cost of transformers

c^{total} Total cost of a network solution

D_{ij} Adjacency matrix of a network

$D^{fix/var}_{i,\phi,t}$ Fixed or variable PV selection binary matrix

E A set of customers with PVs

F_{ij} Slime mold flux

FD Slime mold flux demand

G State estimation gain matrix

H State estimation Jacobian matrix

i Index of nodes (see also j)

ij Index of branches between nodes i and j

I_{ij} Current in a branch

$I_{i,\phi,t}$ Current at a node

I^c Cable ampacity

I^M Arbitrary large current value (big M parameter)

I_i^{neg} Negative sequence current at a node

$I_{i,t}^{R/I}$ Real or imaginary components of current

j Index of nodes (see also i)

k Iteration step

L_{ij} Length of a branch

M Set of PV penetration levels

n Number of nodes

N Set of network nodes

$N^{3\phi PV}$ Set of network nodes with PVs

n^{OLTC} Number of tap operations until maintenance

N^{PV} Set of nodes with PVs

n^s Number of substation nodes

n^{tap} Number of tap operations

n^{TF} Number of transformers

p_i Slime mold pressure

P_{ij} Active power in branch ij

P^0 Transformer no-load loss ratings

P^{Cu} Transformer load loss rating

$P_{i,\phi}^{PV,mrg}$ PV safety margin

P^{TF} Transformer maximum load over a year

P_t^{TF} Transformer power

PD_i Estimated maximum load

PG_i Power generation

r^c Cable resistance

S^{TF} Transformer capacity

T Set of time steps of the reduced power profile

T^l Loss utilization time constant

T^w Set of 1008 steps of a week on 10-minute time resolution

$V_{a/b/c}$ Voltages of phases a, b, or c

V^n Nominal voltage

V^{bg} Background voltage

$V_{j,t}^{R/I}$ Real or imaginary components of a voltage

$V_t^{R/I,bg}$ Real or imaginary components of the background voltage

$V_{i,\phi}^{95\%}$ 95th percentile of a voltage

$V_{j,t}^{-}$ Negative sequence voltage component

$V_t^{-/+bg}$ Negative or positive sequence component of the background voltage

W State estimation weighting matrix

x State estimation vector of the network states

x^c Cable reactance

z State estimation measurement vector

z^c Cable impedance

z^t Transformer impedance

Z_{ij}^{TF} Transfer impedance matrix

γ Slime mold tube decay rate

δ_i Voltage phase angle

$\Delta V_{i,\phi}^{95\%}$ 95th percentile of the voltage estimation error

ϵ State Estimation measurement noise

ε Annuity factor

η Convergence criterion

η Phase angle

θ Lifetime factor

μ Slime mold flow feedback rate

ρ Node density

τ_t Duration of a time instant

Φ Set of phases a, b, c

ω^{LV} Set of LV nodes

ω^{MV} Set of MV nodes

1. Introduction

1.1 Background and Motivation

Due to accelerating climate change and consecutive global warming, the electric power industry got huge attention in the public discussion. As highlighted in the latest report [1], the energy sector accounts for 77% of greenhouse gas emissions. Burning fossil fuels, such as coal, oil, and gas, has led to a 1.1 centigrade increase in the average temperature since the beginning of the 20th century. Such a drastic increase in the world's average temperature causes consequences that can be seen today and become evident to a wider public. Gladly, public demand sparked a political will to solve the issue by diversifying energy generation with higher shares of renewable energy sources and breaking the carbon lock-in of the energy industry [2, 3]. In 2022 the share of solar and wind energy in the generated energy globally accounted for 12% [4]. Moreover, the energy crisis caused by the 2022 Russian invasion of Ukraine accelerated the energy transition of the European Union countries. The new policies entail diversifying energy imports and a drastic increase in local renewable energy generation.

Solar photovoltaic (PV) generation is one of the fastest to roll out renewable energy sources. Due to that reason, the European Commission boosts the adoption of PVs from roughly 200 GW of installed PV capacity in 2022 to 600 GW by 2030 [5, 6]. In Finland, the adoption of solar power has been stagnant in the early years of the renewable revolution. Perhaps due to the northern geographical location of the country, the general opinion on solar energy was skeptical. However, in recent years the industry saw a rapid growth by adding 60% of installed PV capacity in 2022, reaching 635 MW of small-scale plants, and is expected to grow further [7]. Large-scale PV plants are expected to grow sixfold in the coming years, based on the connection applications [8]. Such growth numbers hint that the industry is just at the beginning of the transition. The historical adoption of other technologies, such as automobiles, mobile phones, and infrastructure like

railroads, followed an S-shape curve. Along the curve, the growth rate is high at the beginning of the adoption and retains a high pace until the end of the transition, when it saturates. The adoption of PV generation is nowhere near the saturation point [9].

The practical utilization of solar photovoltaic technology is inherently decentralized. Technical analyses have shown the benefits of large-scale centralized PV plants [10, 11]. However, the cumulative effect of technical, economic, and other factors has yielded the opposite in practice. It is difficult to scale up PV plants, i.e. build larger photovoltaic plants by combining individual panels. MW-size PV plants are cumbersome to build due to the required large land use and network connection. On the other hand, PVs are easy to scale out, i.e. build many small-scale PV plants. Free real estate for panel installations is commonly found on the roofs of buildings, which are otherwise unused. Also, the presence of a network connection is not an issue as all buildings are connected to a network. As the latest statistics in Finland show, the total installed capacity of large-scale (> 1 MW) PV plants in 2023 has reached 50 MW, which is ca. 8% of the total small-scale PV capacity mentioned above [8]. Similar ratios of large- and small-scale PV plants are in neighboring countries of the region: Estonia and Sweden [12, 13].

Widespread installation of small-scale PV plants to the low-voltage (LV) distribution networks is likely to come with a cost in near future. Some of the networks in the region have recently hinted that the available headroom for additional PV plants is running out. Most noticeably, distribution networks serving sparsely populated areas already try to hinder new installations, for example in Finland [14] and neighboring countries [15, 16]. Such announcements by the network companies are the first red flags for the industry signaling the limited resource for PV installations. Consequently, the term hosting capacity (HC) of distribution networks was coined to study the phenomenon of maximum PV penetration, what are the bottlenecks for the penetration in networks, and how limitations could be avoided in order to increase the installed PV capacity.

1.2 Objective and Tasks

The objective of this dissertation is to investigate the limits of PV penetration in low-voltage distribution networks and further find ways to increase the number of connected PVs. On one hand, the limits are defined by power quality indices and, as a rule, deteriorate if more PV plants are connected to a network. On the other hand, the physical limitations of networks are represented by the ampacity constraints of the network components. The abundant connection of small-scale PV plants to low-voltage networks, often on customer premises sharing one point of common coupling, has

directed the focus of the current study to residential low-voltage networks. The investigation is divided into two main tasks centered around power quality and network structure.

Task 1: Investigate the effect of PV penetration on power quality indices and network component capacity. Furthermore, analyzes which network constraints are most limiting for cases typical to distribution networks in Finland in the presence of high PV penetration. The task is divided into the following subtasks:

a) Develop a tool for stochastic assessment of network states, such as voltages and currents, encompassing load flow function and integrated into a Monte Carlo simulation. This tool enables the generation of probabilistic scenarios of network conditions considering the stochastic nature of load types and PV plant locations. Simulating various network conditions allows to statistically analyze results and consider the 5% violation tolerance.

b) Analyze hosting capacity limiting constraints such as voltage limits, thermal capacities of conductors, and transformer loading. Evaluate which constraints are the most limiting in balanced and unbalanced PV generation scenarios, and which constraints prevail in rural and other network types.

c) Investigate the possibilities for improving the hosting capacity with energy storage, mitigating the unbalance in networks, and network reinforcement. Evaluate the effectiveness of energy storage in reducing the voltage rise by shaving the peak generation. Additionally, investigate how the voltage unbalance is affected by single-phase PVs and how the unbalance could be mitigated. Moreover, compare the costs of reinforcement and compare it to the cost of PV curtailment to find a breakeven point.

Task 2: Investigate the structural aspect of distribution networks and how the structure affects the HC. Find out how the networks should be built in order to accommodate high shares of PV and find the differences between the optimal network design and the networks that were built so far to satisfy the load demand. The task is divided into the following subtasks:

a) Develop a framework to evaluate cost efficient network structure spanning across MV and LV networks for a given set of customer nodes. Divide the customers into LV networks of various sizes and find the losses and network investment costs for each solution. Find optimal network sizes for load-only scenarios and compare them with optimal networks with PV plants.

b) Propose to utilize the slime mold algorithm for network topology generation to serve as a tool for a computationally efficient generation

of greenfield topology designs. Inspired by the behavior of slime mold organisms, this algorithm effectively optimizes network topologies providing an alternative for minimum spanning trees. The algorithm is then utilized in the previous subtask.

1.3 Scientific Contribution

This thesis tries to tackle the two tasks postulated in the previous subsection in a number of scientific articles. This thesis includes eight articles, seven of which are published in peer-reviewed journals and one published in a peer-reviewed conference. The first article conducts a review of the hosting capacity topic and marks the starting point of the HC studies. A larger part of the articles cover Task 1 focusing on the HC limiting constraints, while the scope of the rest of the articles cover Task 2 investigating the network structure impact on the HC. The contribution of each article to the corresponding task is explained below.

Publication I conducts a review on the PV hosting capacity, showing several HC definitions used in the literature and power quality standards applied in different countries. Also, the review provides an overview of HC limiting factors and which are the most common factors in rural and urban networks. Consequently, the review covers HC improvement methods utilized in the literature.

Publication II presents the results of a power quality measurement campaign carried out at low-voltage substations in the Helsinki region, Finland. The measured data is then utilized in further research in two main areas. First, the recorded power quality data shows a starting point for the HC calculations, as the power quality has already slightly deteriorated even before PV plants are connected. Secondly, the measurement campaign provides valuable load demand data for network simulations for the works included in this thesis.

1.3.1 Power Quality

Publication III establishes a Monte Carlo simulation framework for HC assessment. Photovoltaic HC values are presented for several network types and compared to voltage rise limits. Moreover, unbalanced simulations were carried out to reveal the share of single-phase PVs in the network that cause unacceptable voltage unbalance levels. Furthermore, the study includes single-phase storages and voltage unbalance caused by the load to evaluate the resulting HC.

Publication IV presents a comparison of the curtailment of PV generation and network reinforcement. The cost function of the comparison encompasses the capital cost of network components and operating losses in the

network. The article presents a breakeven point when the curtailment becomes less viable, and reinforcement of network components becomes a better solution.

The main focus of Publication V is centered around the VU as a limiting factor of the PV hosting capacity. A convex mixed-integer quadratic formulation is utilized to find the HC of single-phase PVs by maximizing the injected power. Furthermore, the PV phase is changed to a variable to find an optimal single-phase PV connection phase to increase HC and attenuate the existing VU caused by the load.

1.3.2 Network Structure

Publication VI presents a slime mold-inspired network topology heuristic optimization algorithm. It generates a spanning tree topology for a given set of nodes, which is close to the minimum spanning tree (MST). However, the resulting topology is relaxed, avoiding the greedy trap of an MST, while still retaining fast computational time. The results show a comparison of the slime mold algorithm to MST and optimal topologies and demonstrate the benefit of the algorithm by providing a solution balanced between total network length and losses.

Publication VII presents an extensive analysis of the network structure effect on the HC. A given set of load nodes is divided between different numbers of secondary substations to find an optimal ratio of low- and medium-voltage networks. For every division, the slime mold algorithm generates a network, that will be evaluated for the HC for a various number of PV plants. The results revealed the need for a smaller LV network in order to host more PVs. On the other hand, the improvement is on par with commonly used voltage control measures. Furthermore, the analysis showed the development of networks if the average PV power remains the same in the future. If the average PV power remains the same, then the HC will be depleted far before all customers will have PVs.

1.3.3 Practical Implications

The topic of Publication VIII leans towards monitoring low-voltage distribution networks. Distribution networks with distributed energy resources (DER) are simulated with various sets of metering devices and frequencies to collect actual and pseudo-measurements for network state estimation (SE). Furthermore, the estimation error is found in order to evaluate an equivalent PV injection that would cause a voltage rise equal to the error. The PV safety margin calculation is presented to find a limit for PV injection. The article addresses the balance between real-time measurements and network HC that has to be kept in practice.

1.4 Dissertation Outline

This dissertation is organized as follows. Chapter 2 summarizes the results of the literature review on the PV hosting capacity, introduces the basics of the simulated cases, and presents the results of the measurement campaign. Chapter 3 elaborates on the power quality limitations of the HC. It starts with the formulation of the Monte Carlo simulation, describes several simulation cases, and reports the results obtained in the HC studies. Chapter 4 turns to the network aspects of the dissertation. It presents the slime mold algorithm, network structure simulations, and results on the network structure aspects. Chapter 5 dives into the practical implications of distribution network hosting capacity. Finally, Chapter 6 concludes the dissertation and proposes possible future research directions.

2. Preliminary Basics

This chapter collects basic aspects of the thesis that are a foundation for understanding the discussed issues and appear throughout all publications, such as test case networks. Publication I introduce the hosting capacity definitions and calculation methodologies, while Publication II present the power quality and household load data.

2.1 Photovoltaic Hosting Capacity

This section introduces PV hosting capacity definitions and uncovers the results of the HC review. Photovoltaic penetration limits are discussed along with the numbers showing the most pronounced limiting factors.

2.1.1 Hosting Capacity Definitions

The PV hosting capacity is an indication of the amount of PV power that is possible to accommodate in low-voltage networks without violating operating conditions. The hosting capacity can be defined in various ways and the review has shown that the literature is still missing a universally accepted definition. Fortunately, most of the definitions match by accepting the fact that the HC is a ratio and is expressed as a percentage value. During the conducted review a set of various HC definitions was discovered and presented in Table 2.1. Furthermore, Figure 2.1 shows a pie chart with the frequency of the utilized definitions. Around half of the review works defined HC as a ratio of peak PV generation and peak load. Intuitively preferred definition due to the main focus being centered around the load. The main intention is to cover the local demand by local PV generation, and such a ratio is a plausible idea for the usage of PV power. However, it reflects the powers, when the peak of solar generation is in summer, while the peak of demand is in winter. Thus the two actual numbers never meet at the same time. Also, load variations would result in inconsistent HC values. The extension of that definition is the ratio of the generated PV

Table 2.1. Hosting Capacity definitions based on the literature review.

Reference	Hosting Capacity Definition
Peak Load	The ratio of the maximum capacity of the PV installation to the peak load of the feeder.
Transformer Rating	The ratio of the maximum capacity of the PV installation to the transformer's rated capacity.
Customers with PVs	The ratio of houses equipped with PVs to the total number of houses.
Active Power	The ratio of the maximum capacity of the PV installation to the peak active power load of the feeder.
Energy Consumption	The ratio of total annual energy generated by the PV systems to the overall energy demand.
Roof-Space PVs	The roof space of the houses that potentially enable the connection and installation of PV panels.

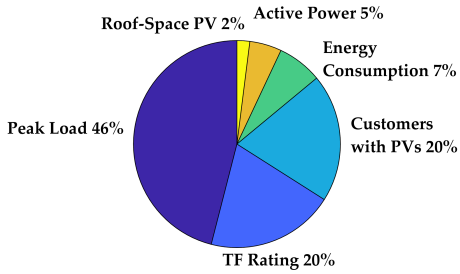

Figure 2.1. Utilized hosting capacity definitions in the reviewed literature.

energy and the demand energy, which overcomes the concurrency issue of the Peak Load definition. Nevertheless, it is not as widely used. The next most popular definition is the Customers with PVs, which accounts for 20% of the review articles. Such definitions have a significant limitation due to the number of houses in the only variable. Usually, each house has a different PV peak power, thus making the definitions misleading. Customers with PVs can be utilized in a narrow niche of cases, where the houses have approximately the same PV peak power. Considering the Active power reference for the HC calculation opens up a possibility to account for the reactive power compensation. It could accompany the Peak Power reference to illustrate the required reserve for the reactive power compensation but would be followed by the same disadvantages. Finally, the Transformer (TF) Rating definition has been utilized in 20% of the cases as well and is the HC reference in the current dissertation. In comparison to the peak load of a network, the TF rating remains unchanged over a significant amount of time. Moreover, the TF Rating has a theoretical limit of 200%, in which case the first half of the PV generation is consumed locally, and the other half is exported to the upstream net-

work. Furthermore, distribution system operators (DSO) generally install secondary transformers of the same sizes on many networks, which gains more insights in an HC comparison of several distribution networks.

2.1.2 Photovoltaic Penetration Limiting Factors

The thesis focuses on slow-changing parameters, such as slow voltage rise and unbalance; cable and transformer capacities. Various other indices, including flicker, harmonics, and public acceptance can constrain the HC as well. The literature review shows the vast majority of the research is done investigating the above-mentioned parameters, reflecting the concerns within distribution networks. Figure 2.2 shows that nearly half of the violations are caused by the voltage rise. Followed by a quarter of the cases of network component capacity violations and a fifth of the cases violating voltage unbalance. The flicker and harmonics are currently not of particular concern.

Voltage Rise

Exceeding the defined performance parameters due to PV penetration can have detrimental impacts on the distribution network operation. Therefore, standardization is crucial for the accurate determination of the HC. Power quality indices, such as the highest voltage level and the highest voltage unbalance, are set in the network standards. There is no global standard nor requirements for network operation, rather countries set standards individually. For example, voltage rise is defined in the European standard EN 50160 as ±10% of nominal voltage (V^n) [17]; American standard ANSI C84.1 as ±5% of V^n [18]; and more restrictive German standard VDE-AR-N 4105 as -5/+3% of V^n [19]. If the first two standards consider the voltage deviation in reference to the perfectly known voltage value, the German standard allows for some leeway. As per the standard, the voltage level on the point of common coupling of a customer with power generating and

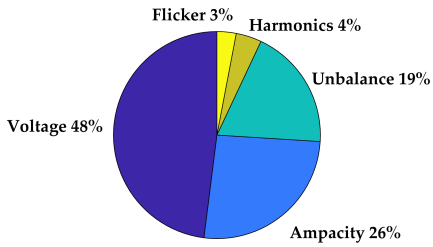

Figure 2.2. Percentages of the limiting factors in the literature showing voltage violations as the most pronounced limiting constraint.

storage units should not exceed 3% of the voltage level without the storage units.

Voltage Unbalance

Voltage unbalance (VU) reflects the asymmetry of the voltage phasors by their magnitude and phase angle. The unbalance factor can be described by several definitions, for example based on the voltage magnitude deviations from the three-phase average value [20]. However, the commonly accepted true definition of voltage unbalance is the ratio of negative $\underline{V}^-$ and positive $\underline{V}^+$ sequence voltage components. The sequence components are obtained by the transformation of the voltage phasors $\underline{V_a}$, $\underline{V_b}$, and $\underline{V_c}$ as shown in the Equation 2.1, where the phasor rotation operator $a = 1 \cdot \angle 120°$.

$$\begin{bmatrix} \underline{V}^0 \\ \underline{V}^+ \\ \underline{V}^- \end{bmatrix} = \frac{1}{3} \begin{bmatrix} 1 & 1 & 1 \\ 1 & a & a^2 \\ 1 & a^2 & a \end{bmatrix} \cdot \begin{bmatrix} \underline{V_a} \\ \underline{V_b} \\ \underline{V_c} \end{bmatrix} \tag{2.1}$$

The voltage unbalance is restricted by the power quality standards as well and the literature review has shown the limit of 1%, 1.3%, and 3%. Finland DSO follows the European standard EN 50160 and sets the limit to 2% [17].

Network Component Capacity

The network component capacity limit is dictated by the component data sheets. Manufacturers give a rating for cables and transformers by evaluating their thermal performance at given test conditions. The test conditions are associated with certain values of ambient temperature, amount of harmonic currents, and several other environment and load-specific aspects while considering the root mean square value of a sinusoidal current. As reflected in the conducted literature review, the capacity limits are often bent towards both more and less restrictive ranges. The review has shown the transformer capacity ranges 100%-150%, while the cable maximum ampacity was 85%-150%. The capacity can be altered in favor of higher HC by reconsidering ambient temperature or force cooling on transformers. Moreover, since the temperature rise due to the electric current is gradual, the capacity constraints can be exceeded for a short period of time. The cable and transformer's physical property of heat capacity prevents the rapid rise in temperature and consecutive deterioration of the insulating materials.

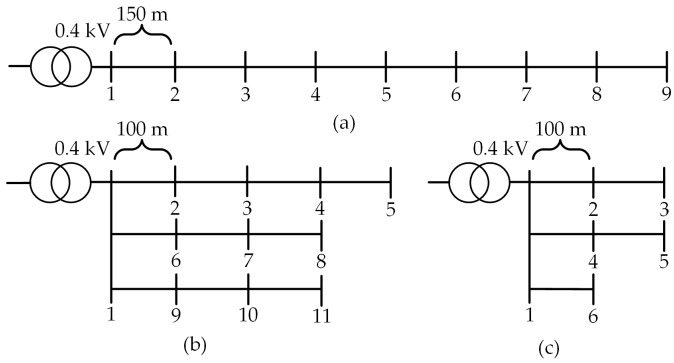

Figure 2.3. Networks modeled in the current thesis for (a) rural, (b) suburban, and (c) urban regions. Numbers denote node indices.

2.2 Test Networks

In the current research, three low-voltage distribution networks are utilized to model the typical conditions in Finland. Shown in Figure 2.3, the networks represent typical networks for rural, suburban, and urban regions of Finland, and were created based on a survey described in [21]. Each region entails a unique topology, feeder lengths, number of customers per node, and the probability of customer heating type. As shown in Table 2.2, the rural network entails the longest feeders among the networks with one customer per node. Such low power density is typical for sparsely populated rural areas. On the other hand, the urban network has short feeders with a large amount of customers per node. Unless otherwise noted, presented networks are utilized for most of the articles presented in this thesis. Furthermore, secondary transformer parameters employed are listed in Table 2.3.

In Finland load profiles of households highly depend on the heating type. As a recent review summarized, residential space heating accounts for two-thirds of energy demand due to the colder climate and is highly correlated with the outside temperature [22]. As shown in Table 2.4, a significant portion of space heating relies on the electric power source.

Table 2.2. Transformer rating and cable parameters of the test networks.

Region	Transformer Rating (kVA)	Cable Type (mm^2)	Ampacity I^c (A)	Impedance z^c (Ω/km)	Cost c^c (€/m)
Rural	50	70	185	0.53+j0.08	32.7
Suburban	200	185	330	0.20+j0.08	54.3
Urban	1000	2×185	2×330	0.10+j0.08	2×54.3

Table 2.3. Transformer parameters (0.4/20 kV)

Region	Capacity S^{TF} (kVA)	Impedance z^t (Ω)	No-load P^0 (W)	Load P^{Cu} (W)	Cost c^t (€)
Rural	50	0.070+j0.11	90	1100	4810
Suburb	250	0.008+j0.02	300	3250	8661
Urban	1000	0.002+j0.01	770	10500	20800

Table 2.4. Household heating types are listed in likelihoods for each region: storage heating, non-electric heating, and direct electric heating.

Region	Storage Heating (%)	Non-El. Heating (%)	Direct El. Heating (%)	Customers per Node
Rural	5.9	52.9	41.2	1
Suburban	7.6	52.5	39.9	4
Urban	0.5	95.3	4.2	60

2.3 Power Quality Survey

During the course of the current study, a power quality survey was conducted. It was carried out in the Helsinki region of Finland during the autumn of 2018. The purpose of the survey was to collect measurement data of power quality indices and high-resolution load waveforms. Collecting such data brings valuable insight into the current state of power quality. Unsymmetrical load and generation contribute to power quality deterioration even before any distributed energy resources are introduced to a network. Considering the above-mentioned power quality limits becomes evident that the so-called headroom for PVs to deteriorate the power quality is smaller, as the power quality stations are not ideal in the first place. For instance, a noteworthy voltage unbalance was observed in all the measured sites due to uneven load of phases. Figure 2.4 depicts a histogram of the VU summed over all the sites, which shows at least 0.4% VU on average. That accounts for 20% of the available HC in terms of voltage unbalance. Moreover, the figure emphasizes the impact of measurement

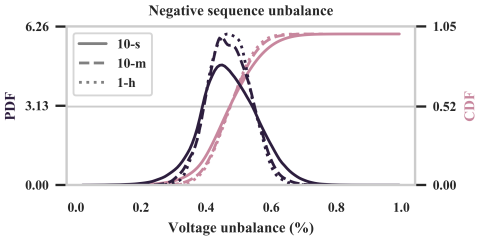

Figure 2.4. Probability and cumulative distribution functions of the negative sequence voltage unbalance collected at all the measurement sites.

resolution on the HC limit. The power standard [17] definition is based on 10-minute average values, but the VU can spike to higher values, which can be observed by comparing it with the 10-second average values.

Another benefit of measured data is providing input data for the simulations of future works. During the survey, three loggers were measuring outgoing feeders of low-voltage substations for a total of eight weeks. Three measured feeders supplied single-family homes, six feeders supplied 5-10 households, and one measured feeder supplied an apartment building with 18 dwellings. The data was collected at a 10-second resolution, providing a strong foundation for slowly changing power quality simulations.

The measured household loads can be summarized by the ratio of mean and maximum current. The ratio resembles the load factor, which is used to evaluate the utilization rate of the electric networks from the demand perspective. Also, the low ratio suggests that the network draws little power on average, making an occasional household appliance load appear as a significant spike in the load profile. Figure 2.5 illustrates the ratios at three data aggregation time resolutions. The left column shows single households and the apartment building on the bottom cell; the right column shows the results of the feeders supplying various numbers of households. At the 10-second resolution, the ratios of single-family households are around 10%, while the ratios of several households are 20-40%. This indicates a lower utilization rate and can be further extrapolated to a lower load factor of networks serving sparsely populated areas. Furthermore, the use of a longer averaging period (10 minutes and 1 hour) of the ratio of mean and maximum currents tends to shave the peaks and concentrate data around the mean value. The ratio of the single-family households increases up to 25% in the case of 1-h, and up to 30-60% for several households. Utilizing longer averaging periods in power systems load

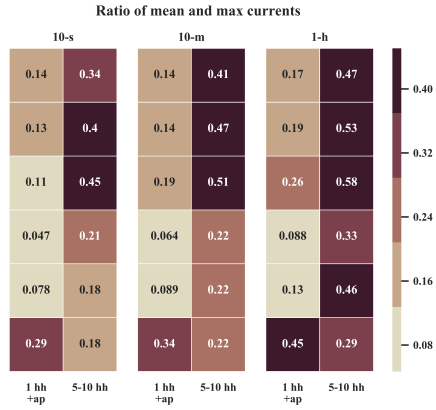

Figure 2.5. The ratio of mean and maximum current of each feeder supplying households (hh) and one apartment building (ap). Three data aggregation time resolutions are presented: 10-second, 10-minute, and 1-hour.

demand not only conceals the peaks in measured load demand but also diminishes insights into the concurrency of these peaks. Understanding the concurrency of load peaks is crucial, especially from the PV hosting capacity perspective, as it compares the capacity margin of power systems and highly coinciding PV generation.

2.4 Photovoltaic Generation

Solar irradiance is utilized to calculate the PV generation power. The formulation is adopted from [23] which accounts for beam, diffuse, and global irradiances; peak power, tilt, and orientation angles of a PV panel; outdoor temperature. The sun altitude angle was calculated based on the solar time, which is a time corrected to the actual location of a PV panel, neglecting the error due to the longitudinal width of time zones. Moreover, the HC studies utilized clear-sky PV generation, which is derived from the physical locations of PV plants, the geometry of the sun and earth, and a predefined diffuse irradiance factor. Current work adopted the clear-sky irradiance calculation methodology from [24], with Linke Turbidity diffuse factor equal to 3. Figure 2.6 illustrates PV power output calculated from the irradiance of a clear-sky case and an actual PV output of the same day.

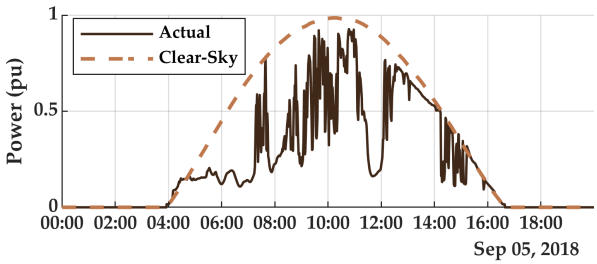

Figure 2.6. Curves of clear-sky PV output and a case of an actual PV output.

3. Power Quality

This chapter presents the methods and results of the power quality aspects of the hosting capacity study. The aim is to identify a niche that has not been studied enough and focus on uncovering it. Publication III introduces the hosting capacity evaluation methodology and presents the base scenario for the results of the rest publications. Publication IV adds network investment and loss costs formulation, Publication V presents the methodology for VU mitigation in the presence of single-phase PVs.

3.1 Literature Review

Photovoltaic hosting capacity assessment has been made so far via simulations of various networks, either using probabilistic or deterministic methods. In real-life networks, HC assessment is limited due to the difficulty of building full-scale test networks, thus it is concentrated on simulating virtual counterparts of existing networks.

Authors of [25] showed an empirical analysis of the HC and how is it affected by PV plant locations and network topology. Among other things, the work proposed to use two hosting capacity values: minimum HC for the case where the violations may begin to occur and maximum HC when violations will likely occur. [26] has studied the impact of high PV penetration on the voltage rise and flicker, and concluded that severe power quality issues will arise if 30% of customers would install average PV plants of 7 kWp.

Stochastic frameworks for HC assessment are the most widely used in the literature. Due to the probabilistic nature of the PV generation, the deterministic approaches can give an incomplete view of the HC. Some of the possible cases can be missed in a deterministic analysis, while the stochastic method, for example, Monte Carlo, can catch all the possible combinations of input variables. In a Monte Carlo simulation, input variables can be randomly sampled from probability distributions, and over the course of many iterations, a statistical result is obtained. However,

the probability distributions of the input variables should be carefully chosen in order to carefully mimic real-life cases. The results can be analyzed by statistical means with much comprehensive picture of the outlier values, average, and other percentiles to find the risk level that the network is willing to tolerate. A Monte Carlo HC assessment is presented in [27]. 1000 iterations were used to randomly sample networks, including PV locations. The numerical analysis presented risk levels of violations based on a statistical analysis of the results. [28] presents a Monte Carlo analysis for a week-long simulation to assess violations as per EN 50160 and evaluate on-load tap changer (OLTC) control strategies. Considering a real low-voltage three-phase network, OLTC with voltage monitoring increases HC the most and keeps the number of tap changes as low as possible. [29] have studied the increase of PV hosting capacity by optimally switching capacitors, adjusting voltage regulator taps, managing controllable branch switches, and controlling smart PV inverters. Various network configurations were sampled in Monte Carlo simulation and HC was found by solving mixed-integer nonlinear optimization problem. [30] used Monte Carlo simulation on 50,000 real LV networks and concluded that 1% of randomly selected networks is enough to accurately evaluate the HC. Moreover, the study included the analysis of the number of PVs in a network, power factor, voltage magnitude on the medium-voltage (MV) system, and conductor impedances. Monte Carlo simulation was utilized in [31] to propose a slightly different approach to quantify PV penetration by using actual building roof data when calculating the PV hosting capacity. This overcomes the possible roof space limitation, which is often overlooked in HC studies. [32] has studied the use of battery energy storage systems (BESS) to increase the HC. A 24-hour rolling horizon-based non-linear optimization is modeled to solve the BESS dispatch.

Numerous works have analyzed the limiting contribution of the VU on the PV penetration with probabilistic frameworks. In [33], authors proposed a simple, yet effective methodology for VU assessment using the transfer impedance matrix. Authors in [34] emphasized the importance of the cumulative duration of violations since the standard sets the violation tolerance on a week basis. The contribution of several VU sources was utilized to prospect possible VU mitigation possibilities in [35] using the Monte Carlo simulation. A probabilistic VU sensitivity analysis in [36] showcased lower VU levels at urban networks, while rural networks fall into severe VU levels. Moreover, traditional Monte Carlo simulations were carried out in [37, 38] to assess VU and its extent to PV hosting capacity. Authors of [39] focused on the contribution of several VU sources on a single node. The Thevenin approach was utilized in [40] to allocate contributors into downstream and upstream (background).

As observed in the reviewed articles above, most of the works set a fixed PV output power and evaluate its impact on the VU. On the other

hand, formulating the tasks as an optimization problem can find a PV penetration such that the VU constraint is met. The true definition of the VU is a division of two complex numbers, and for that reason, the optimization turns into a nonlinear and nonconvex problem. Several researchers tried to employ heuristic algorithms to optimize the HC in the presence of the VU. A study on VU mitigation by EVs with the particle swarm optimization algorithm was presented in [41]. A hybrid method of stochastic optimization, genetic algorithm, and fuzzy logic was proposed in [42]. The genetic algorithm was utilized in [43] to minimize the VU. Moreover, the VU minimization was presented in [44] and [45] as a part of multiobjective distribution network optimization. The majority of the works employed the true VU formulation, thus retaining the nonconvexity, and coupled with heuristic algorithms, could not grant a global solution.

While heuristic algorithms provide a good tradeoff between optimality and runtime, they do not guarantee a global solution. Contrary to heuristics, mathematical optimization grants a global solution for convex problems. By sacrificing accuracy by a little and allowing slight relaxation, the convexity of the problem can be obtained, and thus heuristic algorithms are no more necessary. Moreover, modern computers have shown an increase in computational efficiency and allowed researchers to deploy optimization algorithms based on mathematical programming. To convexify the mode in [46], the VU formulation was relaxed by substituting the voltage positive sequence component by the nominal voltage value, which excluded the division of two decision variables. The model in [47] formulated the VU constraint as a quadratically constrained programming. Authors in [48] presented a mixed-integer nonlinear model, which was then linearized and applied in two-stage optimization for day-ahead operation planning. The negative sequence component is calculated on a branch current basis. The currents are split into real and imaginary parts before they are merged in a quadratic constraint. An alternative VU definition was employed in [49] by finding the maximum deviation from the average voltage of the three phases.

It is vital to keep the true definition of the VU formulation for easier comparison of results. However, a minor relaxation of the definition is required to convexify the problem. Most of the aforementioned articles employed the nominal voltage to substitute the positive sequence component. It is a decent relaxation due to a resulting overestimation of the VU. Instead, the utilization of measured positive sequence voltage would provide a slightly more accurate and real-life relaxation of the VU definition.

This thesis also covers a comparison of the costs of network reinforcement and the value of lost PV generation due to the curtailment. From a DSO's point of view, these are the two extremes of the HC improvement in terms of DSO involvement. Network reinforcement requires DSO's deep involvement and large investments, but has long-lasting effect on

the network. On the other hand, the curtailment can be seen as an easy non-wire alternative (NWA) solution to increase the installed PV power. The curtailment must be compensated by a DSO to cover the loss of opportunity cost of the PV owner. Therefore, optimal curtailment analysis can guide DSOs to compensate with high responsibility. Optimal curtailment analyses, as discussed in [50], reveal that decreasing energy curtailment is beneficial, considering savings obtained through reduced compensation. Curtailment benefits were investigated in [51], finding that dynamically curtailing 5% of yearly feed-in power can double the connection capacity of networks. In the context of utilizing network resources, energy storage systems can be deployed to reduce energy curtailment and raise profit margins for stakeholders, as explored in [52]. Optimal storage systems significantly reduce PV curtailment rates, leading to additional stakeholder profits and reduced financial losses [53]. Distribution system operators can delay network upgrades by strategically curtailing energy during critical hours. [54] explored the economic aspects of curtailment and upgrade combinations. Curtailment is recognized by [55] as an unavoidable revenue loss for PV owners as well as a loss of renewable energy. Moreover, the study compared voluntary and involuntary curtailment, emphasizing the importance of avoiding the escalation of the curtailment compensation costs. [56] showed that the situational awareness of network states is important in order to avoid curtailment without any network violations. A game-theory approach was employed in [57] to find a fair curtailment allocation scheme.

This subsection summarizes the work done on HC assessment. A Monte Carlo framework is presented that was utilized to estimate the HC limited by power quality and network capacities. Cases of PV improvement are simulated utilizing BESS in an unbalanced PV feed-in of the three typical test networks. Moreover, a cost comparison of PV curtailment and network reinforcement is presented to evaluate the increase of the HC. Due to the highly restrictive nature of the voltage unbalance, VU mitigation possibilities are specifically studied as well.

3.2 Hosting Capacity Analysis

The opening section of the thesis presents the HC evaluation method utilized in the research. The presented method acts as a backbone for several works within the current thesis and unifies several topics from hosting capacity calculation, its improvement, and network reinforcement studies.

3.2.1 Hosting Capacity Evaluation Methodology

The hosting capacity calculation can be formulated as an optimization problem, where the PV generation is maximized such that the power quality and network capacity constraints are met. In that case, the PV injected power is a decision variable, while the demand is a given parameter. The objective is to maximize the PV injected power such that the power quality constraints are met. Two essential groups of constraints are (a) the power balance equation, which formulates Kirchhoff's circuit law, and (b) the power flow equations, which, based on Ohm's law, define the relation between electric voltage, current, and power. Even though the power flow equations are not linear, finding the HC can be simplified and formulated straightforwardly. Assuming that the power quality and network loading deteriorate by the increasing injection of PV power and that the output power of all PV plants has to be increased proportionally, creates a simple framework for the HC calculations. In the current study, the trial and error method is utilized to calculate the HC. For a given sample network, the clear-sky PV injected power is incremented by a fixed step until any violations are recorded. The violations are detected after a load flow calculation of the sample network is conducted with the given set of load PV plants. All customer nodes are assumed to have PV plants.

Monte Carlo Simulation

Flowchart on Figure 3.1 illustrates the utilized method for HC calculation. The analysis starts by choosing a region for the analysis and generating 1000 random low-voltage networks. Although the topologies of the net-

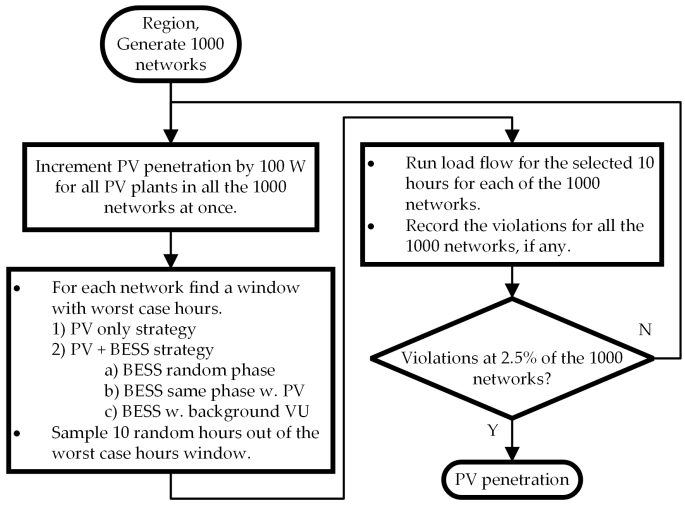

Figure 3.1. Flowchart of the hosting capacity calculation for a network with PV, BESS, and background VU.

works are fixed for each region, the loads are sampled by the likelihood of the heating type. Then, the simulations enter a loop, which increments PV peak power by 100 W at every iteration to increase PV penetration. The first iteration is initialized with a marginal 100 W PV peak power, which is small enough not to cause any violations. The simulation then finds the total power of load, PV generation, and BESS charging power. In order to find the worst possible case, the full power of the BESS is assumed to be available at all hours of the simulation. Figure 3.2a illustrates the search of a worst-case hour for PV only strategy, the simulation constructs a window that covers hours with the lowest total load and highest PV penetration. On the contrary, if a BESS is present at the network, then the window is found at the highest PV penetration and highest BESS charging power, as shown in Figure 3.2b. Next, 10 randomly selected hours from the window are chosen to run the load flow. Such a procedure significantly reduces the search space of the maximization problem. Instead of running the load flow for every 8760th hour of a year, just 10 hours are chosen that will be prone to violations before any other hour. Finally, check if

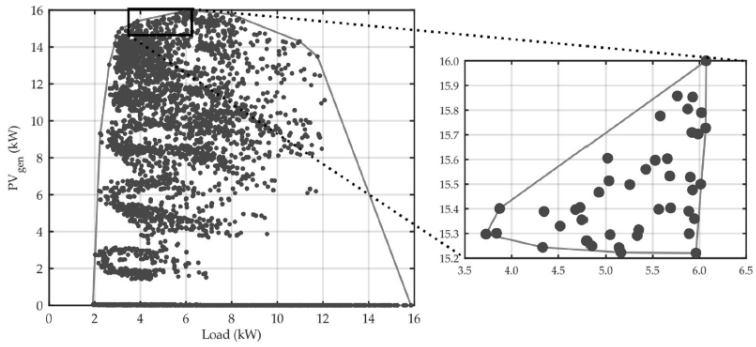

(a) Customers only with PVs.

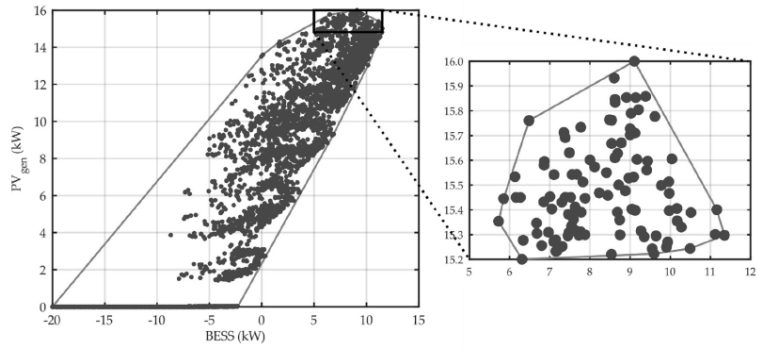

(b) Customers with both PVs and BESS.

Figure 3.2. The window of worst case hours over one year capturing critical hours of the highest PV generation and (a) lowest load, and (b) highest BESS charging power.

any violations were recorded for any of the 1000 networks at the current PV penetration level. If 2.5% of the 1000 networks experienced violations, then the simulation is considered finished, and the PV penetration levels are saved and recalculated to hosting capacity. Otherwise, the simulation returns to the beginning by iterating PV peak power by 100 W and iterating one more time.

Network Reinforcement and Curtailment Cost

In addition to power quality and network capacity limitations, and hosting capacity improvement with home energy storage devices, PV curtailment is investigated as an affordable non-wire alternative for HC boosting. The cost of the curtailed energy is then calculated and compared to a network reinforcement procedure, to find the break-even point, beyond which reinforcing the network becomes viable.

The comparison of network reinforcement and PV curtailment is made on the case networks of the three regions for a given planning horizon. The cost of the network reinforcement is consequently the cost of new cables and/or transformer, and consequently the cost of losses during the operation over the planning horizon. The total cost of a network solution is a sum of costs associated with cables c^{CB} and transformers c^{TF}. Equations (3.1) and (3.2) formulate the cost, which is composed of the following. Cable cost is denoted by c^c, the length of a line connecting nodes ij is L_{ij}, loss utilization time constant T^l, cost of the energy losses c^e, the resistance of the cable r^c and maximum current flow in a branch ij over a year I_{ij}. The total transformer cost over the planning horizon consists of the cost of assigned transformer c^t, transformer no-load and load loss ratings of the transformer P^0 and P^{Cu}, transformer maximum load over a year P^{TF}, and transformer capacity S^{TF}. The operational costs are multiplied by the lifetime factor κ.

$$c^{CB} = \sum_{ij} c^c L_{ij} + \kappa \sum_{ij} T^l c^e r^c L_{ij} 3 I_{ij}^2 \tag{3.1}$$

$$c^{TF} = c^t + \kappa T^l c^e \left[P^0 + P^{Cu} \left(\frac{P^{TF}}{S^{TF}} \right)^2 \right] \tag{3.2}$$

In the current study, the network cables are reinforced based on a rule of thumb rather than an optimization. If any of the nodes will experience voltage rise violation, then the most upstream section (closest to the feeding transformer) of that feeder will be upgraded to the next cable size. If the violations persist even after the upgrade, then the next cable size is considered. If the list of available cable sizes runs out, then the second closest section will be upgraded in the same sequence. The transformers did not have to be upgraded due to their oversizing in the first place. The TF sizes were picked such that they satisfy 20-year load growth and

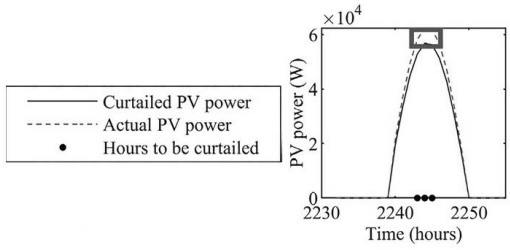

Figure 3.3. Photovoltaic curtailment realized in the current analysis by decreasing PV peak power.

still have 15% headroom left. The list of network components and their costs is shown in the report of the Energy Authority of Finland, which regulates the network component prices for DSOs [58]. Parameters of cables and transformers are taken from well-known manufacturers in Finland: Prysmian [59] and ABB [60].

Similarly, the photovoltaic curtailment is realized by a rule of thumb. As shown in Figure 3.3, the hours with violations are recorded for further curtailment cost calculations. The waveform is then decreased by 1% in steps until no violations. For the hours with violations, the area between the actual PV power and curtailed PV power represents the curtailed energy. The annual curtailed energy is calculated by summing up the curtailed power over the hours that the curtailment was necessary over one year. Then, the total curtailed energy is multiplied by the feed-in tariff of 0.05 EUR/kWh to find the total cost of the curtailment. Finally, the total cost of curtailment is compared to the cost of reinforcement. If the curtailment is cheaper, then the PV generation is incremented by the fixed step. The cost comparison of the curtailment and reinforcement is repeated until the costs reach the breakeven point.

3.2.2 Case Studies and Simulation Results

Several case studies are presented to cover possible real-life examples, which include PV-only cases with all three-phase PV, all single-phase PVs, and varying percentages of single- and three-phase PVs. Then, three cases with energy storage are presented, including BESS connected to a random phase, connected to the same phase as a PV, and finally added background voltage unbalance.

Hosting Capacity

This subsection presents the results of the initial HC investigation. It covered three- and single-phase PV generation. During the investigation a ratio of single-phase PV was found, which causes unbalance violations, and was further extended to include BESS.

	Three-phase PVs		Single-phase PVs		Mixed PVs		
Region	Violation	HC (%)	Violation	HC (%)	1-ph. PVs (%)	Violation	HC (%)
Rural	Volt. rise	105	VU	25	10	VU	63
Suburban	TF	110	VU	58	25	VU	103
Urban	TF	108	Neutr. amp.	41	-	-	-

Table 3.1. Hosting capacity (HC) of three- and single-phase PV cases. Also, a mixed PV case is shown with the ratios of single-phase PVs, which causes the unbalance violations. Hosting capacity as % of transformer rating.

Table 3.1 summarizes the HC in PV only scenario. Several phase connection cases were modeled to find the HC of the two extremes: three- and single-phase PVs. The main limiting factor for the HC in the rural network is voltage rise, while the suburban and urban networks are prone to transformer capacity limitation. The HC values are around 100% of the feeding TF. If all the PVs were single-phase, then the HC would drop 2-4 times, reaching values of 25% in rural, 58% in suburban, and 41% in urban. The VU and neutral wire ampacity would rise as the most common violations. Such a drastic drop in HC is alarming and to investigate the impact of unbalanced PV generation, the share of single-phase PVs was increased until the occurrence of the voltage unbalance violation. The share of single-phase PVs was increased in steps of 5%. A relatively small share of single-phase PVs cause the VU violation, with a significant drop in HC. Especially in the rural network, where a 10% share causes a nearly 40% drop of HC. The violations caused by single-phase PVs in the urban networks do not result in the VU violations, but the neutral wire overload, and due to that reason are not shown in the table. Furthermore, Table 3.2 summarizes the simulation results of the cases with BESS and background voltage unbalance. In case BESSs are connected to random phases, then the HC is not improved as expected by the energy storages. If the BESS and a PV are in different phases, the excess generation can not be absorbed by the storage. The combination of randomly connected single-phase PV

Region	Battery Phase	Single-phase PVs (%)	Violation	HC (%)
Rural	Random	5	VU	23
	Same	50	VU	115
	Same + Backg. VU	50	VU	111
Suburb	Random	10	VU	81
	Same	80	VU	170
	Same + Backg. VU	80	VU	164

Table 3.2. Hosting capacity (HC) of the mixed PV case with BESS. Three BESS strategies are shown: BESS connected to random phase, same phase with PV, and additionally introduced background VU. Hosting capacity as % of transformer rating.

and BESSs is a source of high unbalance, which is reflected on the low HC values. However, if the BESS and PV are in the same phase, then both the HC and share of single-phase PVs are increased significantly, bringing huge benefits to the household. The HC can be increased by fivefold in the rural network, and two times in the urban network. Including the background VU indeed lowers the HC, but the decrease is marginal. This can lead to a conclusion that the background VU has a minor impact as compared to the unbalance from the local DERs.

Network Reinforcement Against Photovoltaic Curtailment

This results subsection presents a comparison of two HC increasing strategies: network reinforcement and PV curtailment, in addressing network cost-efficiency challenges. Figure 3.4 shows that PV curtailment is more cost-effective at the very beginning of the violations. However, a single-time upgrade can give larger headroom to incorporate PVs in contrast to curtailment where curtailment percentage has to be carefully controlled for all the PVs equally. Results show that the rural region has a larger

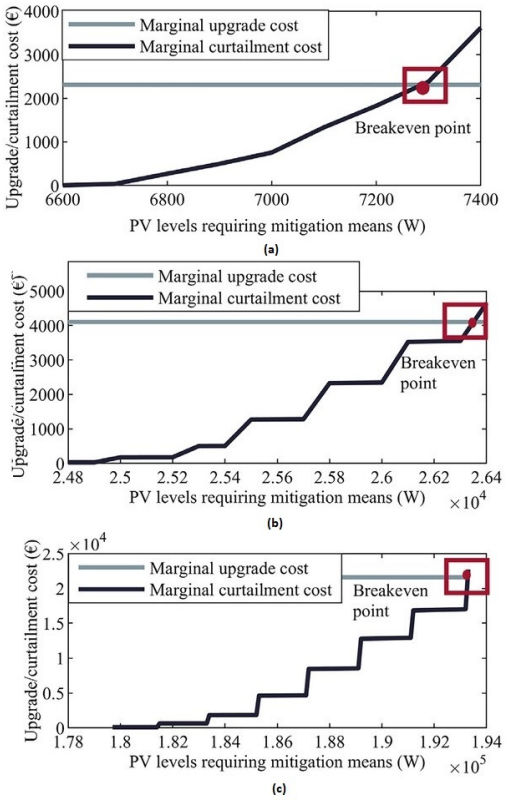

Figure 3.4. The cost comparison of the network reinforcement and PV curtailment for the three regions (a) rural, (b) suburban, and (c) urban.

potential of using curtailment to improve HC as network reinforcement cost is higher due to several reasons, such as longer lines, single-feeder configuration, and frequent voltage rise violations. This can be confirmed by the breakeven point at around 7.3 kW, which is approximately 12% higher than the initial HC of the network of around 6.4 kW. Compared to suburban and urban networks' breakeven points, which are reached at around 26.3 kW with 7% increase and 193 kW with 8% increase respectively. In contrast, the upgrade cost in the suburban and urban regions is comparatively lower to remove network violations due to a three-feeder configuration and node distribution among three feeders. Since the feeders are shorter than in the rural network, reinforcing one feeder section has a higher impact on the network performance.

3.3 Voltage Unbalance Mitigation

The results of the hosting capacity analysis have shown that the VU applies strict limitations if even a small number of single-phase PVs is introduced to a network. This subsection presents the work on the mitigation of the VU in low-voltage distribution networks with single-phase PVs. First, it presents a mathematical formulation for a mixed-integer quadratic programming (MIQP) task to solve the voltage unbalance conditions. Then, the results present VU mitigation by single-phase PVs and the calculation of the PV HC constrained by the VU.

3.3.1 Proposed Voltage Unbalance Optimization Model

This section proposes an optimization model to minimize the VU and maximize PV penetration contained by the VU. The formulation is based on the transfer impedance matrix and a key assumption that the negative sequence current injected into a network by a single-phase PV equals ⅓ of the total output current. The output power of a PV plant is assumed to be equal to a single-phase circuit to 16 A, which corresponds to ca. 3.7 kWp. This power value will be further referred to as the single-phase circuit capacity.

Transfer Impedance

Transfer impedance is a network impedance model and is utilized to calculate the contribution of each PV plant to the negative sequence voltage. As presented in [33], it consists of i by j matrix, that transfers the injected current of a PV plant at node i into the voltage drop at node j. Each element of the matrix represents the impedance between the slack bus and the point of common coupling for two nodes. The negative sequence

voltage, as a sum of background and PV-caused negative sequence voltage, can be found as follows in Equation (3.3).

$$\underline{V}_j = \sum_i \underline{Z}_{ij}^{TF} \cdot \underline{I}_i^{neg} + \underline{V}^{\mathrm{bg}} \qquad j \in N,\ i \in N^{\mathrm{PV}} \tag{3.3}$$

For nodes i and j, the $\underline{V}_j$ is total negative sequence voltage, $\underline{Z}_{ij}^{TF}$ is a cell of the transfer impedance with a mutual impedance of nodes i and j, $\underline{I}_i^{neg}$ is PV-injected negative sequence current, $\underline{V}^{\mathrm{bg}}$ is background negative sequence component obtained from measured voltage waveforms, N is a set of network nodes and N^{PV} is a set of nodes with PVs. Note that the variables presented are phasors, and constitute magnitude and angle values.

Convex Formulation

The model shown in (3.3) is further extended into a quadratic programming (QP) formulation. The connection phase of a PV plant is treated as a parameter at first. Later, the phase selection is changed into a decision variable and together with the PV injection current decision variable, forms a mixed-integer quadratic programming model. Both of the formulations are presented with two objective functions: maximize PV injection and minimize VU. Maximizing PV can be portrayed as finding HC. Even though HC calculations generally consider more constraints than just VU, the presented model can be interpreted as PV hosting capacity with respect to VU. The objective function encapsulates the total sum of PV injection at all nodes with PV, at any phase and any time, denoted in Equation (3.4).

$$\max \sum_i \sum_\phi \sum_t I_{i,\phi,t} \tag{3.4}$$

Subject to

$$I_{i,t}^R = \sum_\phi \cos\theta_{\phi,t} I_{i,\phi,t}$$
$$I_{i,t}^I = \sum_\phi \sin\theta_{\phi,t} I_{i,\phi,t} \tag{3.5}$$

$$V_{j,t}^R = \sum_i \left[r_{ji}^c I_{i,t}^R - x_{ji}^c I_{i,t}^I \right] + V_t^{R,\mathrm{bg}}$$
$$V_{j,t}^I = \sum_i \left[r_{ji}^c I_{i,t}^I + x_{ji}^c I_{i,t}^R \right] + V_t^{I,\mathrm{bg}} \tag{3.6}$$

$$\sum_\phi I_{i,\phi,t} = \sum_\phi I_{k,\phi,t} \tag{3.7}$$

$$V_{j,t}^{-} = (V_{j,t}^R)^2 + (V_{j,t}^I)^2 \tag{3.8}$$

$$V_{j,t}^{-} \leq 2\% \, V_{t}^{+\,\mathrm{bg}} \tag{3.9}$$

$$I_{i,\phi,t} \leq I^{\mathrm{M}} D_{i,\phi,t}^{\mathrm{fix}} \tag{3.10}$$

$$j \in N, (i,k) \in N^{\mathrm{PV}}, \phi \in \Phi, t \in T^{\mathrm{w}} \tag{3.11}$$

The PV-injected current is split into real and imaginary parts, as shown in (3.5). The real phase angle values $\theta_{\phi,t}$ are fixed parameters and are given by measured phasor data. Thus, the cosine and sine functions are both constants, that are scaling the injected current value by the phase and angle of voltage phasors. In (3.6), the real and imaginary parts of the negative sequence voltage are calculated, reflecting the contribution of a single PV plant, with the background-measured voltage component. The condition of equal PV contribution is enforced by Equation (3.7). It is assumed that all PVs are in close vicinity and they are exposed to the same amount of irradiance. The real and imaginary parts of the negative sequence voltage are merged back in the quadratic equation (3.8). The negative sequence voltage magnitude is limited to 2% of background positive sequence voltage in (3.9). To avoid the division of two variables and keep the convexity, measured data are utilized in the VU denominator. Such relaxation is fair, as the true positive sequence voltage tends to increase during PV generation. The obtained values of the presented formulation are smaller, thus staying on the safe side and underestimating available headroom for PV injection. The big-M concept is applied in (3.10) to limit injected current to zero in case of phases that have no PV plants. The I^{M} is an arbitrarily large positive value. The sets are defined in (3.11) and are valid for all the equations presented above. All presented variables are non-negative.

The convexity condition is granted by the linearity of voltage components. Real and imaginary parts of the negative sequence voltage are found as a linear function of the decision variable $I_{i,\phi,t}$ (PV-injected current). The sum of squared linear functions is convex, hence the problem is convex and the global solution can be found.

The VU minimization problem is based on the constraints presented above, except for the objective function. As shown in Equation (3.12), the objective function is the sum of negative sequence voltages at every node and all time instances.

$$\min \sum_{j} \sum_{t} V_{j,t}^{-} \tag{3.12}$$

Subject to (3.5)–(3.11)

The phase parameter is now changed to a free binary variable, which converts the problem into MIQP. The binary variable $D_{i,\phi,t}^{var}$ adds to the complexity of the problem. The objective function, however, remains as compared to the previous case and is maximizing the total PV current

injection, as in Equation (3.13).

$$\max \sum_{i} \sum_{\phi} \sum_{t} I_{i,\phi,t} \tag{3.13}$$

$$\text{Subject to (3.5)–(3.9)} \tag{3.14}$$

$$I_{i,\phi,t} \leq I^{\mathrm{M}} D^{\mathrm{var}}_{i,\phi,t} \tag{3.15}$$

$$\sum_{\phi} D^{\mathrm{var}}_{i,\phi,t} = 1 \tag{3.16}$$

$$j \in N,\ (i,k) \in N^{\mathrm{PV}},\ \phi \in \Phi,\ t \in T_{\text{l-h}} \tag{3.17}$$

While the majority of the equations remain the same, the phase selection variable causes changes in the set of constraints. As previously, the big-M concept is utilized in (3.15) to restrain current from reaching positive values in phases without PV connection. Condition in (3.16) holds if a PV plant at node i is connected only to one phase ϕ. The set of the time interval is changed to two time instances in (3.17). All newly introduced variables are non-negative. Due to the high computational complexity of mixed-integer tasks, the time interval set consists of the time instance with the highest and the lowest background VU, as compared to the fixed phase case, where the time interval covers a full week on 1008 10-minute values. The VU minimization problem holds little changes compared to the previous formulations and consists of previously prepared equations 3.18.

$$\min \sum_{j} \sum_{t} V^{-}_{j,t} \tag{3.18}$$

$$\text{Subject to (3.14)–(3.17)}$$

Monte Carlo Simulation

The evaluation of VU mitigation is realized by the Monte Carlo simulation as well, however is slightly modified as compared to the previous case study. The simulation starts by sampling input variables: the number and the locations of PVs. All customers have the same probability of having a PV plant. The number of PVs is sampled from a lognormal distribution built on the statistical summary presented in [61]. The study states that the average power of a PV plant in Finland is 6 kWp and the median is 4 kWp. The ratio of average and mean is projected to the standard deviation. With the acquired mean and standard deviation, a lognormal probability distribution function is built, assuming that 30% of households have PV plants installed on average. The assumption is based on the conclusions of the [61], which shows the profitability of PV is feasible at 30% of the residential building stock in the Helsinki metropolitan region. Furthermore, one week of the background VU is sampled from the set of

measured data and additional deviation of voltage magnitude and angle is added to the measured data. Voltage unbalance is then calculated for the following PV phase connection strategies.

- Strategy 1—Random phase
  PV plants are connected to a randomly sampled phase among the phases a, b, and c with equal probability.
- Strategy 2—Sequential phase, starting with phase a
  PV plants are connected in a sequential order a-b-c-a-...
- Strategy 3—Sequential phase, starting from random phase
  The starting phase of the phase sequence is sampled randomly. The sequence then follows the same pattern as in strategy 2.
- Strategy 4—The phase with lowest voltage
  The phase with the lowest voltage is estimated by the negative sequence voltage phasor. The angle of the negative sequence voltage phasor is compared to the angles of the phases and the phase with the highest angular difference is chosen as the connection phase.

Input parameters, that were sampled in the previous step, are kept the same for all the strategies. Voltage unbalance is calculated for each 10-minute time step of one week. Then, a 95th percentile value of each node is calculated with the highest VU value is then saved for result analysis. During the third step of the Monte Carlo simulation, the optimization routine is initiated. Since the PV injection value fluctuates over a week, the most conservative minimum value is chosen at first to represent PV injection. However, to take into account the tolerance condition allowed by the standard, the 5th percentile value of PV injection is found at each node and then saved for further analysis. The flowchart of the simulation can be seen in Figure 3.5.

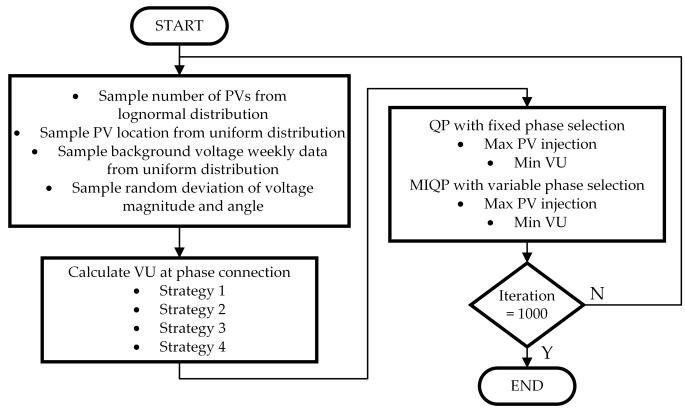

Figure 3.5. Flowchart of the Monte Carlo simulation assessing VU mitigation.

3.3.2 Case Studies and Simulation Results

This subsection presents the VU assessment by Monte Carlo simulation and VU mitigation by the MIQP formulation. Due to the low VU levels in suburban and urban networks, the optimization showcases only the rural network.

Photovoltaic Fixed Phases

The results of the QP formulation are presented with PVs connected as per phase connection strategies. The histogram of the maximum PV injected current can be seen in Figure 3.6. As expected, strategy 1 performs worse than strategy 2 and 3, because sequentially connected PVs balance each other. Strategies 2 and 3 perform quite similarly, except for the bump around 20–25 kW for strategy 2. Starting the phase sequence at phase a at all times (strategy 2) will guarantee good results in part of randomly generated scenarios. Strategy 4, however, demonstrates the worst performance. The reason behind the bad results is the changes in the negative sequence voltage vector. The phases of strategy 4 are fixed in the case where PV injected power is equal to the single-phase circuit capacity at a particular background VU. However, if the injected power of PV plants is increased, the relative contribution of background unbalance to the resultant unbalance vector is decreasing. By increasing injected power even further, PV plants must rearrange connection phases to mitigate increasing unbalance caused by themselves. Phase selection must be reconsidered every time after the power is altered. The results of minimizing the VU at fixed phase connection are shown in Figure 3.7. The histogram of VU attenuation is shown in (a), where it can be seen, that attenuation is hindered by the phase selection of strategy 3 and strongly depends on the background VU phasor. Because the phasor angle is fixed to the feeding voltage phasor, the attenuating vectors of single-phase PVs are not able to follow the vector of the background VU, and the attenuation is not always possible, as indicates the average attenuation

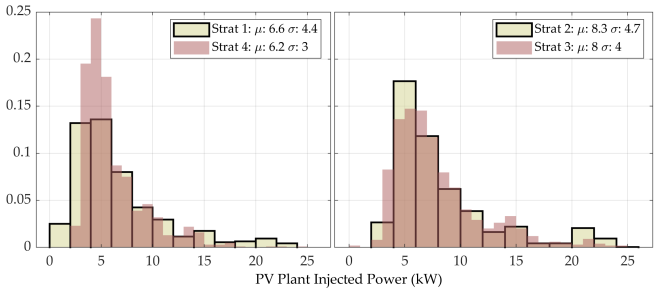

Figure 3.6. Maximum PV injection at fixed phases.

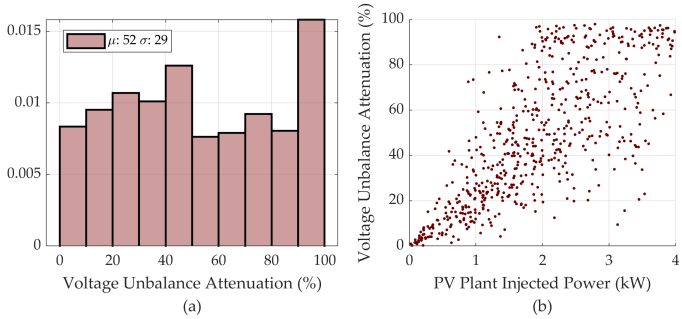

Figure 3.7. Voltage unbalance attenuation at strategy 3 (a) and corresponding PV injection (b).

value of 52%. As compared to other results of the current study, voltage unbalance mitigation subject to fixed phases is the only case where some iterations yield no improvement. Voltage unbalance was attenuated in 69.1% of the cases generated in the Monte Carlo simulation. The VU attenuation with respect to PV injected current is shown in (b). A vague linear relationship can be noticed between the attenuation and injected power. Within successful iterations, the single-phase circuit capacity was able to minimize VU in 85.6% of the tries. Full attenuation of VU can be achieved at relatively low power values.

Photovoltaic Variable Phases

Next, the problem formulation is altered by introducing a binary decision variable for PV phase selection, increasing the computational complexity. Due to that reason, the results below are found for two time instances: the lowest and highest background VU over a week. As can be seen on Figure 3.8, optimal phase selection results in high PV injection powers. The average value of injected current is nearly double that of strategies 2 and 3 in Figure 3.6. In comparison with high background VU, the average value of injected current at low background VU is smaller. The reason is that more PV power is directed toward VU mitigation. The peak injection

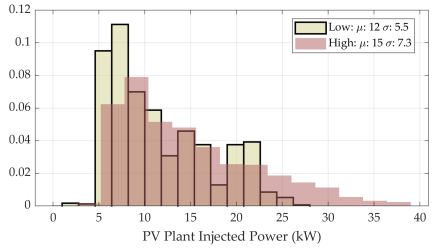

Figure 3.8. Maximum PV injection at optimal phase selection.

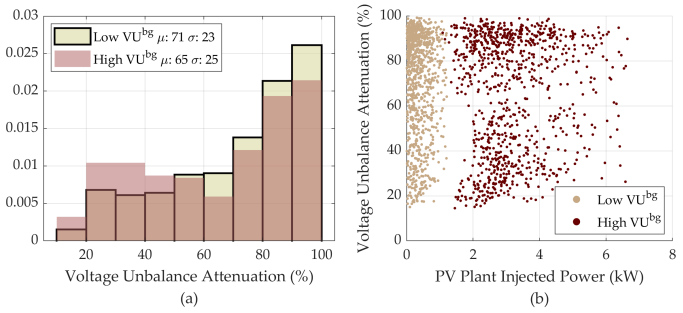

Figure 3.9. Voltage unbalance attenuation with optimal phase (a) and corresponding PV injection (b) at the lowest and highest background VU

reaches values as large as 35 kW. VU attenuation at the variable phase is shown in Figure 3.9, where (a) reveals, that despite the higher injected power shown in the figure above, the average VU attenuation is lower at high background VU. In contrast to the fixed phase, the VU is attenuated to a higher extent at variable phase selection. Additionally, optimal phase selection results in VU attenuation at all times, as none of the instances on subplot (b) are within close vicinity of 0% attenuation, as compared to Figure 3.7b. Moreover, the attenuation is achieved at minor power injections: 99.9% of time instances with the lowest background VU were attenuated by the power lower than the single-phase circuit capacity. The highest background VU was attenuated by the single-phase circuit power in 71.7% of the simulated iteration.

3.4 Chapter Conclusions

In summary, this thesis presented a Monte Carlo simulation with a worst-case hour selection to evaluate photovoltaic hosting capacity in low-voltage distribution networks. It was further upgraded with a network reinforcement method, that facilitated a comparison with the curtailment of PV output powers. An MIQP model was presented to optimize the phase selection and power injection of PV plants. The simulated test networks include rural and urban regions of Finland, with a mix of electrically and non-electrically heated household load demand.

The results indicated specific challenges in distinct network regions, showing the rural network as susceptible to voltage rise violations and urban areas to network capacity limitations. Energy storage systems installed at the same households with PVs increased the HC significantly, by absorbing the excess PV generation during low demand. Furthermore, the simulations with unbalanced PV feed-in cases highlighted the critical impact of the single-phase PVs on the VU increase and thus decreasing hosting capacity. Even a modest share of single-phase PVs causes a pro-

nounced reduction in the HC, raising concerns over the future development of household PV installations. The topic of the voltage unbalance was investigated further to find promising outcomes of the possible VU mitigation. The problem was formulated as an MIQP problem and solved with a PV phase connection as a variable. A strategic selection of the PV connection phase has been shown to mitigate the most severe VU by as much as 3.7 kW PV plants. However, connecting PVs into phases sequentially as $a, b, c, a...$ etc. holds the VU on acceptable levels. Finally, a comparative assessment between PV curtailment and network reinforcement clarified the cost-effectiveness of curtailment in scenarios with a small number of violations, while network reinforcement demonstrated superior effectiveness if the HC is desired to be increased beyond 7-12%, depending on the region.

4. Network Structure

This chapter presents the network structure analysis and its impact on the hosting capacity. Publication VI introduces the slime mold algorithm - a heuristic algorithm that is shown to be employed for network topology generation. Publication VII leverages the slime mold algorithm to generate numerous network topologies for the analysis of the network structure and PV hosting capacity.

4.1 Literature Review

Through the literature review conducted, it was observed that a myriad of studies focus on PV impact on power quality, but some HC aspects of the network structure remained mostly unstudied. The works on that topic covered operational optimization, network reinforcement, and expansion of current networks. That could be explained by the high cost of the reconstruction of distribution networks, which leads to the locked-in state of network structures. However, knowledge of optimal network structures in the presence of high PV penetration could provide insights into future networks. Greenfield network topology design is a backbone for generating new network structures and optimal operation with distributed PVs.

A major challenge with greenfield designs is an enormous number of possible connection combinations. Network meshing designs can be employed to narrow down the feasible region of greenfield planning tasks, for example, the Delaunay triangulation, which creates predefined connection paths between the nodes. The steepest descent and simulated annealing optimization are shown in [62] to find a topology within mesh-like candidate connections. A triangular mesh initialized the bacterial foraging optimization algorithm in [63]. The dynamic programming method is used to find an optimal topology within candidate options in [64], followed by a relocation of some nodes to improve the objective value. A street grid can be considered as a meshed structure for optimization initialization, as it was demonstrated in [65]. Furthermore, authors in [66] and [67] have

optimized network structures in the presence of distributed PV generation. All the works considered pre-defined candidate connections as decision variables, which reduced the search space for the optimization solver. [66] employed the genetic algorithm to solve a mixed-integer non-linear programming problem of accommodating fluctuating renewable generation. Nevertheless, the test case consisted of a small network with predefined connections and two candidate locations for substations. [67] employed the biogeography-based optimization algorithm to solve an MV/LV network planning problem.

Several works constructed connections within LV networks by directly connecting each node to the closest substation via straight lines, i.e. start topology. As shown in [68], that is the most computationally efficient method but is the farthest from real-life network construction practices. An MV/LV network planning was shown in [69] utilizing the imperialist competitive algorithm to optimize the location of the HV substation and MV network topology in one formulation. However, the authors narrowed the search space significantly by fixing LV substation locations. Analysis in [70] had fixed locations for PVs and other DERs. The optimal number of microgrids was analyzed for deterministic and probabilistic planning approaches, while the number of local generation units remained unchanged. Load nodes were divided into LV networks in [71] to represent different numbers of substations for a given planning area. The results revealed the optimal sizes of LV networks and an MV/LV network ratio.

The minimum spanning tree is easy to understand and implement, but it minimizes only the length of a network. The other crucial components of the total cost, such as loss costs and others, are neglected. Despite that disadvantage, it was employed in numerous other works in network optimization. A genetic-based algorithm in [72] used the Prüfer sequence chromosome coding, which entails a population set of feasible spanning trees. Works presented in [73, 74] have utilized an MST to create a set of feasible network topologies as initial populations for genetic algorithms. In [69] a multistage expansion planning algorithm employed an MST to construct a radial MV network of the distribution network optimization. A comprehensive network planning was presented in [75], by addressing network planning in an MV/LV design. The k-means clustering algorithm was used to partition load nodes into LV networks and then generate the topology for each network by the MST. A similar approach was demonstrated in [76] by generating MST topologies for LV networks partitioned by the k-means algorithm. However, distributed generation plants were allocated to candidate locations. Still, the study concluded that considering both MV and LV networks in the optimization is beneficial in the presence of distributed generation. The optimization method proposed in [77] spatially clustered load nodes into groups by similar load. The topology within each cluster is then found with MST based on reliability requirements.

Several algorithms can be employed to find an MST, for example, Prim's or Kruskal's algorithms. An MST can be extended to find Steiner trees, as shown in [78]. However, just a few attempts to improve the MST hint that it satisfies most of the tasks.

Concluding the review literature, the work presented in this thesis focuses on an optimal structure as a ratio of MV/LV networks with respect to increasing PV generation. A given set of load nodes is partitioned into varying numbers of LV networks, which reflects the number of loads served by one substation and, consequently, the split of LV and MV networks in the electricity distribution. For each MV/LV solution, the hosting capacity and the cost of networks are found. In order to find the topology of the solutions, a new topology-generating algorithm is presented - the slime mold algorithm. The proposed algorithm demonstrates the advantage of MST relaxation. The resulting topologies are a step back from the greedy approach of the MST and illustrate the balance between the shortest and star-like networks. It fills the gap in the algorithms that do not require candidate connections and can manage an enormous search space in reasonable computation time.

4.2 Topology Generation

This section presents an algorithm for a network topology generation for a greenfield design of a large-scale distribution network. The proposed algorithm generates topologies closely resembling minimum spanning trees but avoids the greedy trap and demonstrates the advantage of a relaxed MST.

4.2.1 The Slime Mold Algorithm

A distribution network can be defined as a set of interconnected nodes consisting of load and substation nodes. Each node has parameters such as index i, x- and y coordinates, and estimated maximum load PD_i. The connections between two nodes i and j are denoted in an adjacency matrix D_{ij}. The number of nodes is denoted by n and the number of substation nodes by n^s. Except for rural areas, networks are built in a meshed structure. However, they are operated in a radial topology and the unused links are utilized as back-ups. In the current study, the total cost of a network consists of two parts: investment and loss costs, as shown below.

$$c^{total} = c^{inv} + c^{loss} \tag{4.1}$$

$$c^{inv} = \varepsilon \sum_{ij} c^c \, L_{ij} \, D_{ij} \tag{4.2}$$

$$c^{loss} = \varepsilon \, \kappa \sum_{ij} c^e \, T^l \, r^c \, L_{ij} \, 3 \, I_{ij}^2 \tag{4.3}$$

Table 4.1. Network cost parameters for the Slime Mold Algorithm analysis

Parameter	Symbol	Value	Unit
Energy loss cost	c^e	5×10^{-5}	EUR/Wh
Loss utilisation time	T^l	2000	hour/year
Cable resistance	r^c	1.82×10^{-4}	Ω/m
Cable cost	c^c	75	EUR/m
Cable ampacity	I^c	365	A

The investment cost (4.2) includes the annuity factor ε, connection length L_{ij}, cable cost c^c and binary directed adjacency matrix D_{ij}. The loss costs formulated in Equation (4.3) include annuity as well as the lifetime factor κ, cost of energy losses c^e, loss utilization time T^l, cable resistance r^c and current flow I_{ij}. The rest of the simulation parameters have generalized realistic values based on the authors' experience in network planning in Finland, and are listed in Table 4.1. For a more detailed description of ε and κ, please refer to [79].

Slime Molds and Application Areas of the Algorithm

The algorithm is inspired by the behavior of a slime mold organism *Physarum polycephalum*, which is a large yellow single-celled organism that can be found in cool and moist locations. Once deployed on a plane, it starts to grow outwards in search of a food source. The growing slime spreads around, covering the searched area with a thin layer of slime. After it finds a food source, the slime is concentrated around it in a thicker layer. Once two or more food sources are found, the slime mold forms a tubular network with conducting tubes to transport nutrients throughout the entire organism. Thicker tubes are formed between the food sources, while the slime in previously explored areas decays. The remaining tubes have been proven to connect food sources via shortest paths [80].

Slime mold gained significant attention when it was demonstrated that it can solve a maze by neglecting dead-ends and choosing a shorter path from several alternative ways [81]. A study conducted in [82, 83] discovered that the slime mold algorithm can construct Steiner trees. The construction of a Steiner tree is an important network optimization problem that is similar to the construction of the MST. Furthermore, the slime mold algorithm was utilized for the optimization of numerous transportation networks. Remarkable results have been accomplished in modeling the Tokyo railway system by [84, 85]. A clever utilization of the algorithm led to stunningly close-to real-world network performance in terms of routing and fault tolerance. Similarly, the modeling of motorway networks in [86] has shown results similar to existing networks. Supply chain optimization by the slime mold algorithm was introduced in [87], and the load shedding of electricity demand by the slime mold was studied in [88]. The analogy of

slime mold and electric power networks was briefly presented in [89] but was never unfolded.

Mathematical Formulation

The model is based on the food transportation within the slime mold between the food sources via tubes. The tubes conduct fluid with nutrients from node i to node j, which is pushed by the pressure difference p_i and p_j. The resulting flux of the fluid F_{ij} flows through the tube with conductivity D_{ij} and length L_{ij}. Then, as in [81], we have

$$F_{ij} = \frac{D_{ij}}{L_{ij}}(p_i - p_j) \tag{4.4}$$

The nodes in the system are classified into two types: sink nodes and source nodes. Sink nodes signify the load nodes, whereas source nodes signify the substation nodes. Each sink node has a flux demand of FD and each source node supplies to the system the total demand divided by the number of source nodes. Over the course of simulations, the flux demand value was set to $FD = 0.2$. However, the effect of the flux demand value on the result still requires further analysis, as some applications alter the value and treat it as an input parameter [90]. According to Kirchhoff's law, the total flux at each node is conserved, keeping the net flux at the rest of the nodes equal to zero. The balance of flux between several source and sink nodes is defined in Equation (4.5) [87]:

$$\sum_j F_{ij} = \begin{cases} \sum_i FD_i/n^s & \text{, if } i = \text{source} \\ -FD_i & \text{, if } i = \text{sink} \\ 0 & \text{, if } i = \text{rest} \end{cases} \tag{4.5}$$

The adaptive network formation was described in [81] by the difference Equation (4.6). The tube conductivity reacts to the flux by gradually shrinking the tubes without flux and expanding the tubes that are conducting flux. Flow feedback rate μ and tube decay rate γ are the input parameters. The tube thickness response is calculated at each iteration k by:

$$D_{ij}^{k+1} = D_{ij}^{k} + \left(\left| F_{ij}^{k} \right|^{\mu} - \gamma D_{ij}^{k} \right) \Delta k \tag{4.6}$$

A system of linear equations is formed by equations (4.4) and (4.5) for all the nodes and tubes. The pressure p-values values are obtained by solving the system of linear equations at every iteration k. Furthermore, by securing the pressure value for reference nodes $p_{source} = -1$, the solution of (4.4) will result in a unique pressure value for every node. Assuming that tube conductivity and its length constitute a matrix $A_{ij} = \frac{D_{ij}}{L_{ij}}$, an auxiliary matrix B_{ij} from Equation (4.7) can be used to reconfigure of its diagonal

and off-diagonal elements.

$$B_{ij} = \begin{cases} -A_{ij} & \text{, if } i \neq j \\ \sum_j A_{ij} & \text{, if } i = j \end{cases} \tag{4.7}$$

Then, using B_{ij} the vector of nodal pressure values can be solved by using the backslash operation in MATLAB as shown in (4.8):

$$B_{ij} \setminus FD_i = p_i \tag{4.8}$$

The simulation is initialized with tube conductivities D_{ij} equal to one. During the simulation, the conductivity values of decaying tubes will converge to zero and tubes that survive foraging will converge to a positive value. All the tubes that converge to a positive value constitute an undirected adjacency matrix of the final topology. A summarizing flowchart of the algorithm is depicted in Figure 4.1. Slime mold solution requires calculations over a range of iterations k to converge the pressure matrix. Once the pressure difference between the previous and current iteration is lower than η, the slime mold algorithm is considered to have converged (4.9):

$$\frac{\left|p_i^k - p_i^{k+1}\right|}{p_i^k} \leq \eta \tag{4.9}$$

Parameter Exploration

Flow feedback rate μ and tube decay rate γ are the input parameters that should be explored in order to find a balanced solution. As mentioned before, the slime mold algorithm solution converges towards an MST. However, by relaxing the parameters, the topology can step back from the MST (Figure 4.2a) towards the star topology (Figure 4.2c). A balance between the smallest total length and smallest loss costs can be achieved as shown in Figure 4.2b. Typically, a desired result corresponds to a rather

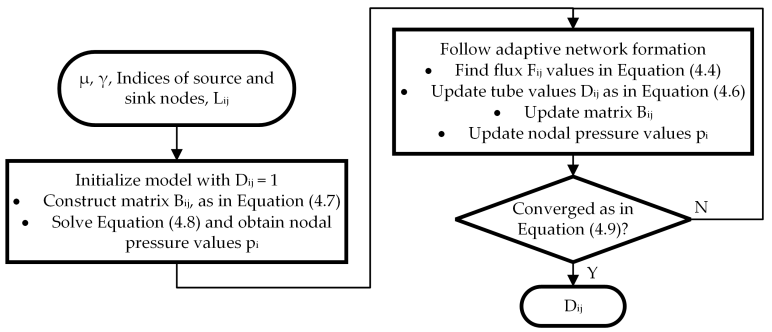

Figure 4.1. Flowchart of the slime mold algorithm.

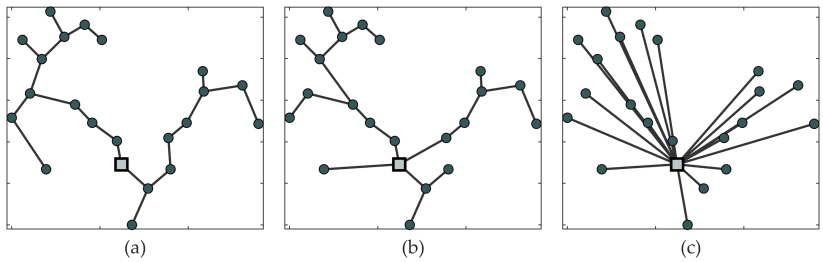

Figure 4.2. Topology types for the same set of nodes (a) MST, (b) Slime Mold solution, and (c) Star topology.

high μ and low γ, while the intervals of the two are $1 \leq \mu \leq 5$ and $0 \leq \gamma \leq 1$. Values of μ lower than one will prevent the model from convergence, leaving many alternative connections between sink and source. Exceeding the upper bound will result in breaking some of the node connections, leaving some of the sink nodes disconnected. The tube decay rate has an opposite effect on the slime mold dynamics. A value of γ around the upper bound will result in a star topology with direct connections between source and sink nodes. By decreasing γ, the network topology will gradually approach the MST. The heatmap of the total cost dependency on the input parameters can be seen in Figure 4.3a, where the cost is normalized by the cost of the MST of the network shown in Figure 4.2. The NaN values on the top-left corner of the plot indicate that the model did not converge. The split of normalized costs of the previously considered network can be seen in Figure 4.3b. Considering one cable size, network investment costs increase linearly with total length, while the loss costs have a nonlinear relationship with length. Loss costs are lowest in star-like topologies and increase abruptly near the MST. Typically, the lowest cost is close to that of the MST, but not exactly. In the current test case, the optimal network cost is nearly 20% lower than that of MST due to the very high loss costs.

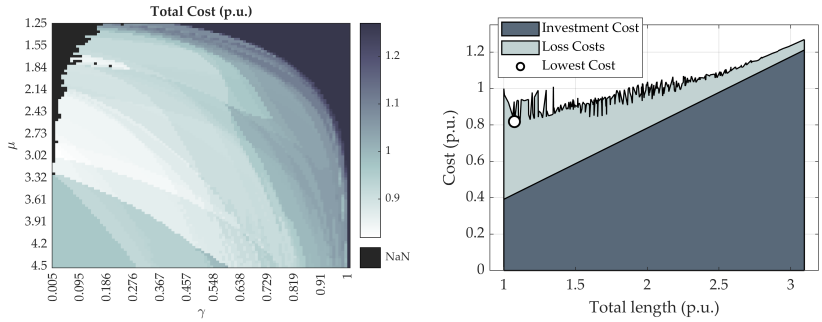

(a) Heatmap of the total cost dependency on the input parameters μ and γ.

(b) The network total cost split between investment and loss costs.

Figure 4.3. Cost function values of the Slime Mold Algorithm solutions.

Sector Based Slime Mold

Clustering the load nodes into pie-chart-like sectors ensures the cable ampacity of the solution is not violated. The number of clusters is determined by preventing a feeder load from exceeding the cable ampacity I^c. The k-means method starts with one cluster and increases until the feeder capacity is not violated, achieving a balanced load distribution among the feeders. After clustering, the slime mold optimizes each sector independently, shaping the final network topology.

4.2.2 Comparative Simulation and Results

The simulations are carried out on synthetic networks, which are randomly generated sets of nodes for rural, suburban, and urban areas. The scale of network area, number of nodes, and estimated average loads follow typical Finnish networks described previously. Load nodes are clustered by the k-means clustering method into a number of clusters that is equal to the number of substations, where the centroids represent substation locations. Table 4.2 includes the parameters of the synthetic networks. Other algorithms such as Prim's algorithm, mathematical programming, and a Network Planning Algorithm (NPA) developed in Aalto University [91] are utilized to provide a performance comparison of the slime mold algorithm. The Prim's algorithm is a well-known way to generate an MST. Prim's algorithm entails the greedy approach, which means that the next decision is made based on the smallest cost among available options. It is simple to implement and fast to simulate.

Following is a mixed-integer quadratic programming formulation that illustrates the global optimum. Due to its high computation time, the MIQP is only applied in the case of rural networks with a low number of nodes. The current study relies on the simplified model of the power flow equations presented in [92]. The objective is to minimize the total cost function of Equation (4.1), while the formulation of constraints is as

Table 4.2. Network parameters for the slime mold algorithm tests.

Network Type	Number of Nodes	Number of Substations $\boldsymbol{n^s}$	Span of Network (m)	Estimated Load PD (kW)
rural	6 11 16	1	1200	10
suburban	41	1	400	11
urban	301 602 903	1 2 3	$200 \times \sqrt{n^s}$	8

follows:

$$\min_{D_{ij}} \quad c^{total} \tag{4.10}$$

$$PG_i - PD_i = \sum_j P_{ij} - \sum_k P_{ki} \tag{4.11}$$

$$I_{ij} = \frac{P_{ij}}{v} \tag{4.12}$$

$$I_{ij} \leq D_{ij} I^{\mathrm{M}} \tag{4.13}$$

$$\sum_{ij} D_{ij} = n - 1 \tag{4.14}$$

$$PG_i = 0, \text{if } i = \text{sink} \tag{4.15}$$

D_{ij} is a binary directed adjacency matrix and I^{M} is a big M constant, PG_i is the power generated at node i, PD_i the power demand at node i, P_{ij} the power transfer from node i to j, I_{ij} the current flow from node i to j, and v the nominal voltage (assumed to be equal for all nodes). All variables, except for the binary variable D_{ij}, are continuous positive variables. Equation (4.10) formulates the minimization of the network total cost. Equation (4.11) enforces active power balance at all nodes: the net generation at a node should be equal to the net export from the same node. The current at every branch is calculated by (4.12). The limit for current flow in a line is set by (4.13). In case the connection is absent, $D_{ij} = 0$, then the current flow is restricted. Otherwise, the constraint is relaxed by the big M, and the current can pass. The numerical value of M is set to be equal to $M = 2\sum_i PD_i$. The radiality constraint is enforced by (4.14). Equation (4.15) restricts power generation at load nodes, leaving the power generation to substation nodes only. For the sake of simplicity, a unity power factor is assumed.

Results of the Rural Networks

The results of rural networks are shown in Figure 4.4, where costs are normalized by the corresponding result of the Slime Mold sector. At a small number of nodes, all algorithms and their variations show comparable cost values. The MIQP model, representing the global minimum, consistently reaches the lowest cost in all cases, as well as on average. Slime mold produces less optimal networks when compared to Prim's MST. In the smallest network size, typically the optimal topology matches the MST, and the slime mold relaxation of the MST does not yield any advantages. However, as the number of nodes in a network increases, the benefits start to be apparent. Additionally, the efficacy of initial solutions for such small networks is questionable, as modern computers and optimization tools can efficiently reach the global optimum within a reasonable time.

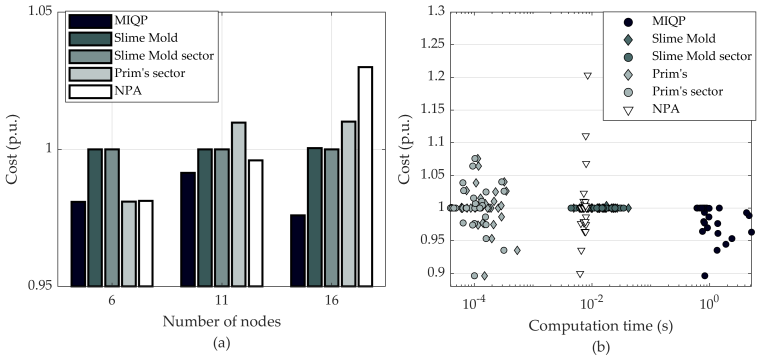

Figure 4.4. Average cost of rural networks (a), and the cost and the computation time of each network (b).

Results of the Suburban Networks

The suburban networks consist of 41 customer nodes, which is double that of rural networks. At that scale, the advantage of the sectored slime mold becomes evident, as illustrated by Figure 4.5a. The number of customers in suburban networks is big enough to overload a single feeder, thus the clustering algorithm divides customer nodes into a minimum of two sectors, assigning a feeding cable for each. The disadvantage of MST starts to stand out at this size of networks, as the Prim's algorithm shows a 10% higher cost on average than the Slime mold. The unsectored Prim's algorithm was excluded from the comparison due to poor results.

The MIQP model was left out from the comparison due to its unbearable computation time. As discussed in [92, 93], a noteworthy reduction in computation time can be achieved by accepting a slight offset from the global optimum. In an attempt to reach the global optimum for the suburban networks, the MIQP solver optimized the first test network from the ten test networks. Unfortunately, even after 48 hours of computation, the

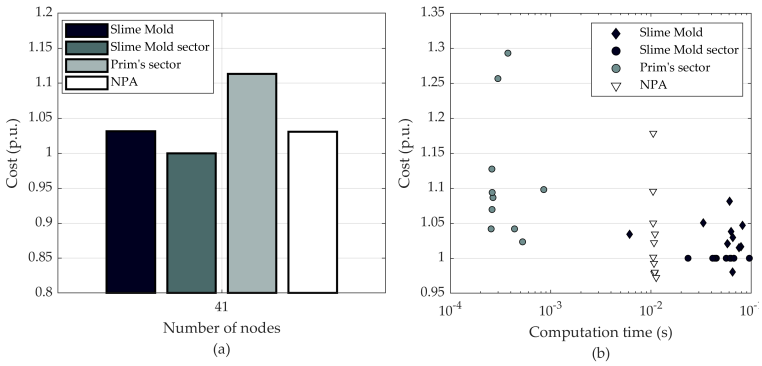

Figure 4.5. Average cost of suburban networks (a), and the cost and the computation time of each network (b).

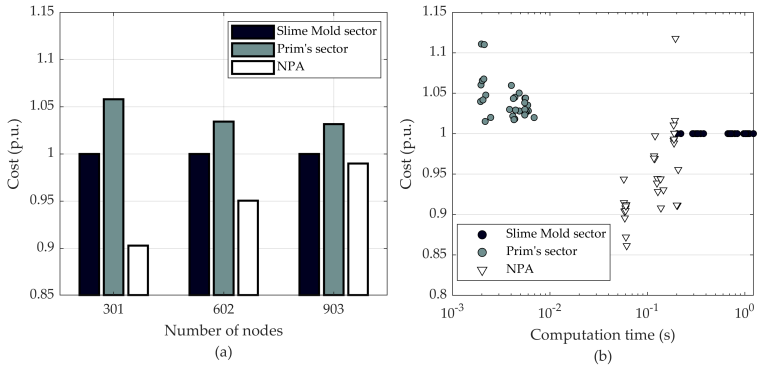

Figure 4.6. Average cost of urban networks (a), and the cost and the computation time of each network (b).

CPLEX solver for the MIQP problem failed to reach the global optimum and stopped at an optimality gap of 5.19%. Nevertheless, the objective value at that stage was lower than any other algorithm, having a value of 95.4% of the sectored slime mold. As shown in Figure 4.5b, the overall trend in computation time for suburban networks mirrored that of rural networks, with both slime mold algorithms performing within a similar time frame, while Prim's proved to be faster.

Results of the Urban Networks

The normalized results of urban networks, as depicted in Figure 4.6, indicate that the sectored slime mold produces a network at 3-5% lower cost when compared to Prim's MST. As the network size increases, the difference in the algorithms becomes less severe. Larger networks pose a challenge to topology generating algorithms and it gets increasingly difficult to comprehend the large number of nodes. The computation time of the sectored slime mold is still higher than the other algorithms: three orders higher than Prim's algorithm and one order higher than NPA. The networks generated by the "pure" slime mold have a cost 50% higher than that of the sectored slime mold, and, therefore, it was left out from the comparison.

4.3 Optimal Network Size

This section presents a summary of the network structure studies and the structure's impact on the PV hosting capacity. The network structure is divided into low-voltage and medium-voltage networks for the delivery of power to end customers. A network-generating methodology, that is used in the HC evaluation framework, is presented. Several results of the

optimal LV network sizes are shown with respect to HC and compared to the most common voltage control measures.

4.3.1 Proposed Simulation Model

The optimality of networks is evaluated by their total cost, which accounts for MV and LV networks, consisting of investment and resistive loss costs of cables and transformers, as shown in Equation (4.16).

$$c^{total} = c^{CB} + c^{TF} + c^{MV,CB} \tag{4.16}$$

The calculation of the cost of the lines (cables) is slightly modified from Equation (4.1) to substitute the loss utilization time T^l with a duration of the time instant t, as shown in:

$$c^{CB} = \kappa \sum_{ij} c^c L_{ij} D_{ij} + \kappa\varepsilon \sum_{ijt} \tau_t c^e r^c L_{ij} 3 I^2_{ij,t} \qquad (i,j) \in \omega^{LV}, t \in T \tag{4.17}$$

$$c^{TF} = \kappa n^{TF} \left(c^t + c^{OLTC}\right) + \kappa\varepsilon \left[\sum_t \tau_t c^e P^0 n^{TF} + \sum_t \tau_t c^e P^{Cu} \left(\frac{P^{TF}_t}{S^{TF}}\right)^2\right] \qquad t \in T \tag{4.18}$$

$$c^{MV,CB} = c^{CB} \quad (i,j) \in \omega^{MV}, t \in T \tag{4.19}$$

The left term of Equation (4.17) entails the investment cost of the line ij, where c^c is cable cost, τ_t is the duration of the time instant t from the set of reduced power profile hours T. The transformer cost is formulated in Equation 4.18 as a sum of investment cost, no-load cost, and load costs. c^t is the cost of a single transformer and n^{TF} is the number of transformers, P^0 and P^{Cu} are TF no-load and load loss ratings, P^{TF}_t is transformer power at t, and S^{TF} is TF capacity. The cost of the MV network is found using the same equation as the LV network in Equation (4.17) but calculated over the set of MV nodes ω^{MV} in Equation (4.19).

Voltage Control

In the current study, three voltage control measures are simulated to compare their cost efficiency with optimal network structure. First, LV transformers are equipped with on-load tap changers, which increases the cost of the TF by three times. The tap range is ±4% and works as follows. If the voltage rise reaches the upper constraint, the tap is set to -4% to lower it. As in [94], the depreciation cost is followed after every tap switch and accumulates into a maintenance cost over the lifespan of a transformer. The maintenance cost caused by the switching is linearly dependent on the number of switching operations in Equation 4.20. The maintenance

cost of an OLTC transformer c^{maint} is 20% of the investment cost, n^{tap} is the number of tap operations of a single transformer, and n^{OLTC} is the maximum number of tap operations without maintenance.

$$c^{OLTC} = c^{maint} \frac{n^{tap}}{n^{OLTC}} \tag{4.20}$$

Secondly, reactive power control (RPC) is applied to all PV plants in an LV network if any of the nodes violate the upper voltage limit. To retain simplicity and fast computation time, the RPC is realized as reactive power consumption which is fixed to 10% of the apparent power of a PV plant. Moreover, the output of active power is also reduced by 10% to quantify the cost of the RPC. Lastly, PV curtailment is applied on a PV plant if the voltage exceeds the limit at the PV node. The curtailment rate is 10% of the PV peak power, while the cost of the curtailed power is c^{curt}=0.01 €/kWh [95].

Proposed Framework

Illustrated by Figure 4.7, the proposed framework uses an exhaustive search of the varying number of substations, PV power, and the number of PV plants. First, the given set of load nodes is divided by the k-means++ function into n number of LV networks, each supplied by a single TF located in the middle of the cluster. After the nodes are partitioned, the slime mold algorithm generates topologies for each LV network and MV topology to tie

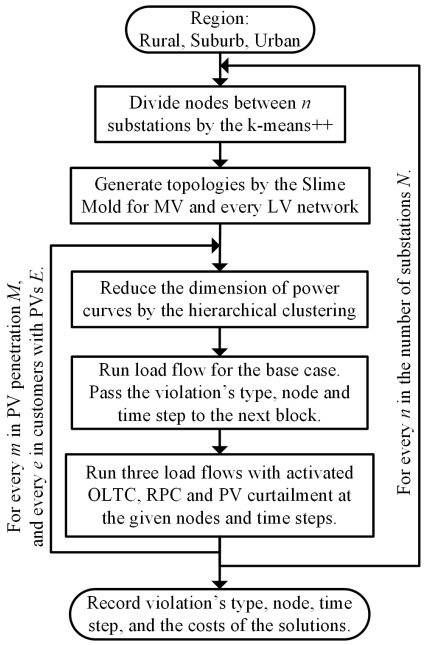

Figure 4.7. Flowchart of the proposed framework

LV substations with the HV substation in the middle of the plane. After the nodes are partitioned, the slime mold algorithm generates topologies to tie customers with LV substations, and furthermore LV substations with a HV substation, which is located in the middle of the plane. Next, the dimension of the power profiles is reduced from 8760 to 1752 hours with hierarchical agglomerative clustering. Finally, the load flow is conducted to evaluate the voltage and ampacity limits in the networks, followed by the evaluation of the OLTC, RPC, and PV curtailment cases. Newton-Raphson-based single-phase AC load flow is utilized to calculate voltage and current levels in the system to evaluate the feasibility of networks on four criteria: voltage drop, voltage rise, cable ampacity, and transformer capacity. In this study, the acceptable voltage deviation from the nominal voltage is ±5%, while the LV network component capacities are listed in Tables 2.2 and 2.3, and the MV network cables in Table 4.3.

The procedure described above is repeated over the three sets. For every $m \in M = \{0, 50, 60, 70, \ldots, 310\}$ which is a set of PV penetration levels measured as a ratio of a peak load. PV output power is incremented in steps as assigned in M. Photovoltaic peak powers are scaled to the ratios of customers' maximum load, to match [61] conclusions that proved the benefit of matching the PV plant size to the load of a household. The current study assumes that customers are willing to maximize PV ownership profits and thus assumes the PV plant dependency on the load size. For every $e \in E = \{0, 5, 10, \ldots, 100\}$ which is a set of percentages of customers equipped with PV plants. PV plants are distributed among the customers with linear interpolation to equally divide PV plants over the simulated set of nodes. Lastly, for every $n \in N = \{50, 55, 60, \ldots, 250\}$ which is a set of the number of substations. In the following text, the term *number of substations* is utilized to reflect the structure of networks. Due to the clear meaning and linear property of the metric, the term is used throughout the current analysis. However, the number of substations is strongly related to the actual size and number of nodes in the network.

4.3.2 Case Studies and Simulation Results

The current study requires minor changes in the case networks. Since many new networks will be generated, a density of the previously presented rural, suburban, and urban networks is taken as a base to extrapolate

Table 4.3. MV cable parameters

Region	Size (mm^2)	Ampacity I^c (A)	Impedance z^c (Ω/km)	Cost c^c (€/m)
Rural	35	210	0.89+j0.38	21.8
Suburb	55	280	0.53+j0.28	25.1
Urban	95	360	0.34+j0.27	29.1

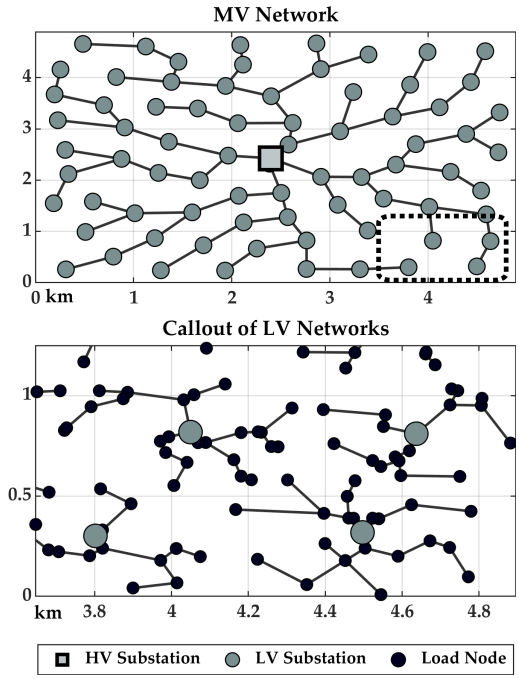

Figure 4.8. The topology of MV network with 75 LV substations. A callout of underlying LV networks of the suburb region.

a larger number of customer nodes. 1500 load nodes are placed in a uniformly random order, covering up a square plane of size $d \times d$, which is based on node density ρ, as shown in Equation 4.21. The node density ρ for the three regions is as follows: $\rho^{rural} = 1200/\sqrt{8}$, $\rho^{suburb} = 400/\sqrt{10}$, and $\rho^{urban} = 200/\sqrt{5}$. Figure 4.8 depicts a network solution of the suburb region. Network topologies are generated with the slime mold algorithm. For the sake of simplicity of the network formation process, a single cable and transformer size is considered for each region [21].

$$d = \sqrt{1500} \cdot \rho \tag{4.21}$$

Optimal Number of Substations

The optimal number of substations is a feasible solution with the lowest cost. Network feasibility is evaluated based on the four criteria of power quality and network capacity outlined previously and a 5% threshold is employed to eliminate outlier solutions and include the tolerance margin [21]. If more than 5% of the networks on the plane have violations, the whole solution is considered infeasible. The total network cost curve and share of networks with violations of the suburb region are shown in Figure 4.9. The same evaluation is applied to rural and urban regions obtaining the following results: rural:suburb:urban = 185:75:160 substations. Note that

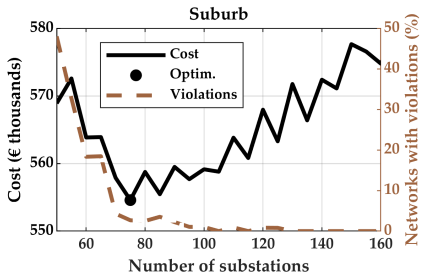

Figure 4.9. Cost and the number of violations dependency on the number of substations in suburb region for the base case

the optimal number of substations is denoted as "Optim." for the rest of the paper.

Voltage Control Against Network Size

The network sizes are compared to commonly used voltage control methods: OLTC, RPC of PV plants, and PV curtailment. Figure 4.10 depicts the effect of the aforementioned methods with the optimal number of substations deviated along the set N in three positive and three negative groups. Each group contains three values ±5,10,15, ±20,25,30 and ±35,40,45 substations. The figure shows the average values of each triplet, where they are denoted by +(-), ++(- -) and +++(- - -) respectively. As indicated in the uppermost subplot, the HC of rural networks would substantially benefit from OLTC, however at a higher cost. Suburban networks represent an intermediate scenario, where both voltage rise and network capacity limit the HC. All the methods contribute to HC enhancement, while the smaller LV networks (higher number of substations) give a comparable increase of the HC as OLTC transformers and RPC. Urban networks face primary issues with capacity constraints, and thus, redistributing loads among more substations, curtailing PV generation, and employing RPC yield the most significant HC improvement.

Highest PV Injected Power

In Finland, a common customer connection is 3x25 A, which is equivalent to approximately 17 kW. The connection size denotes the electric power distributed through it. The connection power is granted by DSOs, and unless stated otherwise, customers are allowed to inject as much power into the network as the connection capacity allows. However, if technical constraints prevent PV penetration before the 17 kW fuse capacity, customers can request DSOs to strengthen the network to enable exporting as much power as the main fuse size, with no additional cost to the customer. Figure 4.11 illustrates that the average PV HC expressed as injected power

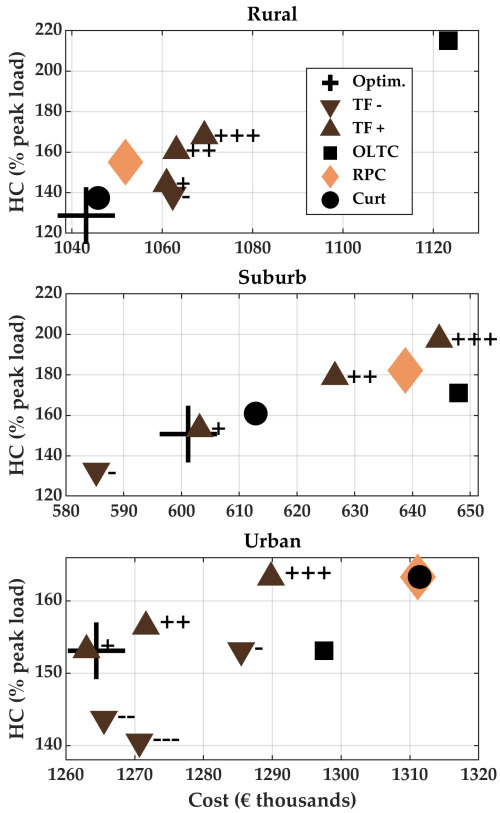

Figure 4.10. Voltage control in comparison to optimal, smaller (TF-) or larger (TF+) number of substation.

in all regions remains well below the connection power limit, typically at only 15-20% of the connection size. Rural and suburban networks can withstand around 2.5 kWp of PV power on average. RPC and curtailment can raise the ceiling up to 2.75 kWp, and OLTC can go even higher. In the urban region, the network's withstand power is the lowest, ca. 1 kWp, and voltage control has limited help. However, the urban area, despite lower individual limits, has significantly more customers per node, making per-customer PV power quite restrictive.

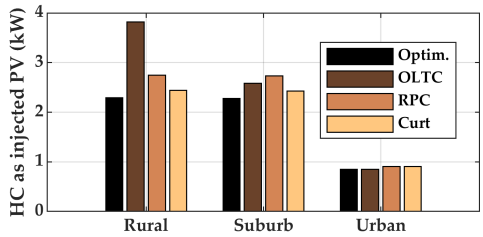

Figure 4.11. Hosting capacity (HC) as average PV injected power per customer.

Current Pace of PV Adoption

Research published in [61] has analyzed the building stock of the Helsinki metropolitan area and concluded that the average PV peak power for residential customers having their own generation is 6 kWp. Moreover, the author of [96] revealed the average PV peak power in one of the DSOs in Finland to be 9.25 kWp. Given the two numbers, the PV penetration is analyzed with respect to the number of customers with PV plants in the following section. Table 4.4 displays the highest feasible proportion of customers with PV installations. In the rural region, up to 25% of customers can accommodate average of 6 kWp PV plants, while a 9.25 kWp capacity reduces the share to 10%. Voltage control measures can twofold the number of customers that would be allowed to deploy PVs. The suburban region exhibits a similar trend, although voltage control measures are less effective in increasing the share of prosumers compared to the rural network. Lastly, in the urban region, the share of customers is the lowest, and voltage control has a negligible effect on the outcome. However, once again the small share of customers can be attributed to the significant difference in the number of customers per node.

4.4 Chapter Conclusions

This chapter of the thesis explored the impact of network structure on the hosting capacity of PV plants in typical distribution networks in Finland. The network structure was altered by adjusting the number of LV substations for a given set of 1500 load nodes, thus changing the size of MV and LV networks. The study showed the influence of network size on PV hosting capacity. For each simulated network size, a cost was calculated, which considered network line investment costs and loss costs. The analysis for hosting capacity involved two approaches: increasing PV peak power and increasing the number of PV plants for customers until any violations.

An optimal number of substations was identified by finding the lowest

Table 4.4. Maximum feasible share of customers (%) with PV plants if average PV plant sizes are 6 and 9.25 kWp

mean PV	Rural	Suburb	Urban
6.00 kWp	25%	35%	10%
+ OLTC	60%	40%	10%
+ RPC	30%	45%	15%
+ Curt.	30%	35%	15%
9.25 kWp	10%	25%	5%
+ OLTC	30%	25%	5%
+ RPC	15%	25%	10%
+ Curt.	15%	25%	10%

cost on a U-shaped total cost curve for every region. The U-shape is formed by two main factors: loss costs and network line costs. Changes in the unit costs of these two factors from Table 4.1 would result in a change in the total cost curve. For example, an increase of energy loss costs would move the total cost curve to the right, making smaller networks cost efficient. Network sizes were compared to commonly utilized voltage control measures, revealing that rural networks benefit the most from OLTC due to voltage rise dominant violations, while urban networks, facing capacity limitations, gain from curtailment and reactive power control of PVs. Network structure changes were identified as a universal solution to increase the HC for all regions, acting alternatively to network reinforcement. Moreover, the results highlight that the network HC per customer's injected PV power is much lower than the main fuse connection size across all regions. Due to the high coincidence factor of PV generation, PV injected power of full capacity can not be granted for all customers with PVs. Most alarmingly, extrapolation of average installed PV plant sizes into the future suggests the need to downsize average PV plants or impose restrictions on PV plant feed-ins to prevent HC depletion in the future.

The network analysis was possible due to a new network topology algorithm. The proposed Slime mold algorithm can cope with large combinatorial search space and generate topologies for greenfield planning tasks without candidate connections. The heuristic algorithm has shown to be a viable alternative for commonly employed topology types of minimum spanning trees and star topologies, by providing a better solution in terms of line investment and network loss costs.

5. Practical Implications

This chapter presents the work of Publication VIII, which emphasizes the practical side of the hosting capacity. The error of actual and estimated network states is analyzed and a PV hosting capacity safety margin is proposed.

5.1 Literature Review

This section of the thesis tries to shed light on the practical side of the hosting capacity. Due to the increasing share of PVs, continuous monitoring and state estimation of the network states become important to ensure safe operation of PVs within power quality requirements. The presence of intermittent DERs has sparked further discussion on the uncertainty of SE.

Authors of [97] employed the Kalman filter for SE at different steps of PV penetration with 15-minute metering intervals. A Gaussian mixture model was proposed in [98] to capture the variance of pseudo-measured PV generation and estimate the impact of measurement variances on SE accuracy. In [99] authors analyzed SE confidence bounds caused by the measurement and network parameter uncertainty. The authors advocated for safety margins to avoid power quality violations. Few works have discussed the uncertainty of measurements and SE. In [100] the uncertainty was analyzed in en LV network with high shares of flexible resources. A probabilistic framework was utilized to showcase the deterioration of SE accuracy due to an overlay of the uncertainty caused by flexibility sources and the uncertainty induced by loads. Several substation metering setups were simulated but without customer on-site measurements. A few scenarios of measurement uncertainties were simulated by a three-phase four-wire SE algorithm in [101] to show the estimation accuracy of the neutral wire and VU in case of unbalanced PVs. A Monte Carlo framework was presented in [102] to analyze the uncertainty. The study also raises the question of the symmetry of the measurement errors. Real-time measurements cause

normally distributed error with an accuracy of three standard deviations, and it is generally assumed the same for the pseudo-measurements (historical or forecasted data used as measurements). However, it is shown that the error distribution of pseudo-measurements is often skewed. Authors of [103] have also studied the skewed error of pseudo-measurements, and proposed an SE formulation that can cope with any probability distribution of the measurement variance. Research in [104] has shown several metering configurations by utilizing typical load patterns for pseudo-measurements and higher smart meter data sampling frequency. The article underlined the importance of SE accuracy as a mere percent accounts for a significant portion of a voltage control range. Meter sampling frequency and data granularity were analyzed in [105], and also introduced the latency in data transfer derived from the distance from a feeding substation and non-synchronized measured data.

This section investigates the accuracy of SE and proposes a PV penetration safety margin. The PV safety margin quantifies the lost PV penetration due to SE inaccuracy and resulting curtailment of PVs to stay within the limits. Several metering configurations are simulated to evaluate the benefit of improved SE accuracy by deploying extra real-time meters in addition to existing pseudo-measurements.

5.2 State Estimation and the PV Safety Margin

In the current analysis, the high-resolution 10-second measured data is utilized to simulate metering configurations. The original data is downsampled to a range from 10 seconds to 15 minutes and the resulting data of numerous resolutions is utilized to calculate actual network state values, real-time measured, and pseudo-measured values. Actual values of the states are calculated by a decoupled load-flow method and are utilized to find the estimation error by comparing it with the estimated values. The loads are assumed to be star-connected. Real-time measurements are resampled to match the frequency of the SE. Real-time measured values are once again taken from the decoupled load-flow analysis conducted after the load active and reactive values were resampled. The pseudo-measurements are customer load power values that were forecasted from the historical data before SE and are based on smart meter (SM) measurements at a 15-minute frequency. In all the cases, the averaging period of the data is equal to the metering frequency. All the (pseudo) measured data is shifted in time by a random fraction of the measurement period (10-, 30-sec, 1-, 5-, 10- or 15-min), which was sampled by the random number generation function in Matlab with seed 1.

State Estimation

The current study uses a Weighted Least Squares (WLS) state estimation algorithm based on node-voltage polar coordinates, as formulated in [106]. Also, a few key assumptions were made: the networks are fully observable, thus no observability analysis was conducted, meter data is reliable and has no false readings, and network parameters are perfectly known.

The state estimation can be summarized by Equation 5.1 as a process, which assigns the measurement vector z to a non-linear measurement function h of the network states x, and measurement noise ϵ, which is assumed to be normally distributed with zero mean.

$$z = h(x) + \epsilon \tag{5.1}$$

The WLS states estimation minimizes the difference between the estimated and measured values, which is formulated by Equation 5.2, where W is the weighting matrix. Each diagonal element of W is a reciprocal of measurement error variances $W = diag(\sigma_1^{-2}, \sigma_2^{-2}, \ldots, \sigma_M^{-2})$, where M is the number of measurements.

$$\min [z - h(x)]\, W\, [z - h(x)] \tag{5.2}$$

The minimization of the objective function shown above is achieved by iteratively solving Equations 5.3 and 5.4. At each step k, a network state correction Δx^k is calculated, which is then added to the state vector x. Matrix $G = H^T W H$ is the gain matrix, and H is the Jacobian obtained by differentiating the measurement function $h(x)$ at x.

$$\Delta x^k = G^{-1} H^T W [z - h(x^k)] \tag{5.3}$$

$$x^{k+1} = \Delta x^k + x^k \tag{5.4}$$

Column vector 5.5 encapsulates the state variables as node voltage angles and amplitudes, where N is the number of nodes.

$$x = [\delta_2, \delta_3, \ldots, \delta_N, V_1, V_2, \ldots, V_N]^T \tag{5.5}$$

The SE algorithm was further augmented to incorporate current magnitude and angle measurements. The traditional current magnitude measurement formulation in WLS SE is numerically unstable because the current values can not be found at the flat start. The pseudoflow formulation was adopted from [107] which substitutes branch current magnitude measurements with equivalent pseudo power flow measurements. Furthermore, an additional formulation for the current angle is adopted from [108]. It is assumed, that if a branch current angle is measured, then its magnitude is measured as well. This allows to convert the polar coordinate formulation into rectangular coordinates, thus providing numerical stability at the flat start for both the current magnitude and angle measurements.

The optimal meter placement approach employed in the current study is based on the gain matrix G from the SE described earlier, which was proposed in [109] and further enhanced in [110]. Due to the circuit representation property of the gain matrix, it is similar to an admittance matrix of a network Y_{ij}. Node voltage measurements contribute to shunt admittance, that is a diagonal element if G_{ii}, while branch current measurements contribute to branch admittance G_{ij}. By formulating measurements in a unified matrix, the circuit representation of the existing measurements and new measurements can be expressed as a sum of two gain matrices. Thus, the trial-error method can find optimal locations for voltage and current real-time measurements by minimizing the sum of diagonal elements of G_{ii}.

Measurement Variances

One of the advantages of state estimation is the allocation of weights to measurement vector z based on measurement variances: the lower the variance, the higher the confidence of an input. The variances of the current analysis are summarized in Table 5.1. Also, it is assumed that the measurement variances are normally distributed and the accuracy percentage is set to reflect the 99.7% confidence bounds, i.e. errors lie within three standard deviations from the zero mean.

Photovoltaic Safety Margin

The photovoltaic safety margin is an amount of power that is equivalent to the SE inaccuracy. Say, if the PV safety margin is $P^{PV,mrg} = f(\Delta x)$, then Δx is an estimation error of a state, e.g. the difference of actual and estimated voltage magnitudes, that can be mapped to an equivalent PV injection power $P^{PV,mrg}$ by a linear function f. The linear relationship between node voltage squared and PV injected power was demonstrated in [111], and has shown an acceptable accuracy of network HC estimations. To capture the safe operation 95% of the time, the estimation error Δx is the 95th percentile value of the voltage magnitude estimation error.

$$\max \sum_{i,\phi} P_{i,\phi}^{PV,mrg} \tag{5.6}$$

Table 5.1. Measurement variances for pseudo-measurements, reference PV (RPV), and real-time voltage and current measurements

Pseudo-measurements	Reference PV	Real-time measurements
The variance of the historical load data P_i for every 15-min time step of a day.	3% of the RPV power output reading RPV_i.	1% of voltage and current readings V_i, I_k.

$$P_{i,\phi}^{PV,mrg} \frac{Z_{ij}^{TI}}{V_{i,\phi}^{95\%}} \leq \Delta V_{i,\phi}^{95\%} \tag{5.7}$$

$$P_{i}^{PV,mrg} = P_{j}^{PV,mrg} \tag{5.8}$$

$$i,j \in N^{3\phi PV}, \quad \phi \in \{a,b,c\} \tag{5.9}$$

The task can be formulated as a linear optimization problem, where the objective is to find the highest PV margin as shown by Equation 5.6, where $P_{i,\phi}^{PV,mrg}$ is the PV safety margin for every node with a PV i and phase ϕ. Equation 5.7 limits the PV margin by the voltage magnitude estimation error. Z_{ij}^{TI} is the transfer impedance matrix, which links voltage drop at node j with current injected at node i, $V_{i,\phi}^{95\%}$ is the 95th percentile voltage of phase ϕ at node i, and $\Delta V_{i,\phi}^{95\%}$ is the 95th percentile of the voltage error. Equation 5.8 limits PV output powers to obtain the same value. Equation 5.9 defines the sets. All the nodes ij are defined over a set of nodes with PVs, N^{PV}, and phase ϕ covers three phases.

5.3 Case Study and Simulation Results

The SE accuracy is evaluated only for the rural and urban networks because they represent two opposite extremes. Various metering scenarios presented in this study differ by the number of smart- and real-time meter configurations. However, all of the scenarios consist of the base setup, which is augmented by additional meters.

The base setup implies pseudo-measurements generated from collected SM data of active power for all customer nodes for each phase, a constant power factor of 0.98, and the voltage at the feeding transformer node $i = 1$ is real-time measured.

Smart meter configuration:

- Setup A1. Reference PV is used to modify pseudo-measurements generated from SM recordings. The nowcasted PV generation is subtracted from the SM forecast obtaining the expected value of the load. If the expected load is negative, then it is changed to zero. After that, both the expected load and nowcasted PV generation are SE inputs for the SE as pseudo-measurements.

  To generate the nowcasted generation of PV plants, a small RPV array is simulated, which is located at a subsection and whose power output is real-time measured. The RPV allows extrapolation of PV generation to PV arrays located in close vicinity by utilizing the ratio of clear-sky and actual PV generation measured by the RPV [112].

Real-time measurement configurations:

- Setup B1. Current magnitudes are measured at each outgoing feeder with PV, i.e. rural network branch locations $ij = \{1,2\}$ and urban network branches $ij = \{1,2\};\{1,4\}$.
- Setup B2-5. Various numbers of voltage (V) and current (I) meters deployed to optimal locations. The numbers of real-time meters are as follows: B2 - 1 V and 1 I meter; B3 - 1 V and 2 I meters; B4 - 2 V and 1 I; B5 - 2 V and 2 I meters.

In the PV margin analysis, the peak power of the PV panels is 9.25 kWp per customer, the power is divided between the phases equally. PVs are located at nodes $i = 5,7,9$ in rural and $i = 2,5$ in urban networks. The tilt and orientation angles are [35°, 50°, 45°] (measured from the norm of a horizontal plane) and [15°, -10°, 0°] (0° facing south).

The load data was split into two halves: one week of training data and one week of simulation data. A well-known time series forecasting algorithm ARIMA is utilized to generate pseudo-measurements for load nodes. An ARIMA configuration presented in [113] was implemented by the Matlab function with parameters ARIMA(2,0,1)(2,0,1)$_{\mathrm{h}}$, where h denotes the number of time steps to count for 24 hours, e.g. in case of 15-minute smart meter data h = 96 of the seasonal period. The prediction is made at every time step of the simulation for one step ahead.

Estimation Error

The results of the estimation error reveal a change in skewness along the values of the states. For example Figure 5.1 illustrates the voltage magnitude estimation error of the rural network. The average taken over time of the voltage magnitude estimation error tends to turn from

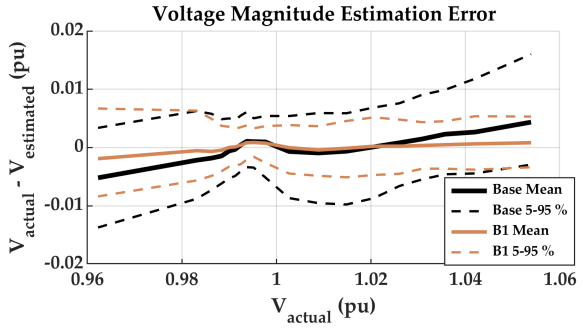

Figure 5.1. Average and 5-95th percentile values of the estimation error of rural network in balanced condition. The base case has only pseudo-measurements and voltage real-time measurement at the feeding transformer; setup B1 implies an additional current magnitude real-time meter at the transformer.

negative to positive as the estimated voltage gets higher. Additionally, a comparison between the base case and measurement setup B1 highlights that additional measurements in the network reduce the skewness and variance of the error. The observed trend suggests that the safety margin of network operation should be considered at higher network state values, specifically, values close to limitations. The error of the whole voltage range can in fact be symmetrical, and thus would lead to the underestimation of the safety margin.

Photovoltaic Safety Margin

The following demonstrates the PV power safety margin due to the estimation error at different metering configurations and frequencies in Figure 5.2. In the rural network base setup, the PV margin reaches a significant 23% of the PV penetration in order to stay within voltage rise limits. Since all pseudo-measurements remain at the 15-min mark despite the SE frequency, the PV margin keeps a high value. Additional real-time meters (B1-B5) lower the margin remarkably even at the lowest metering frequencies. Setup B1 demonstrates a higher margin as compared to the cases with current (B2, B3) and voltage (B4, B5) meters at optimal locations. Voltage meters provide the best accuracy as cases B4 and B5 with two voltage meters have the lowest margin. However, the accuracy gains can be considered minor compared to the extra number of meters that have to be deployed, gaining up to a 5 percentage point reduction of the margin. In the base case, the margin in the urban network reaches 11%. When additional real-time meters are installed, the margin reduces by half in case of a 15-minute SE period and four times in case of a 10-second SE period, similar to the reduction in the rural network. As compared

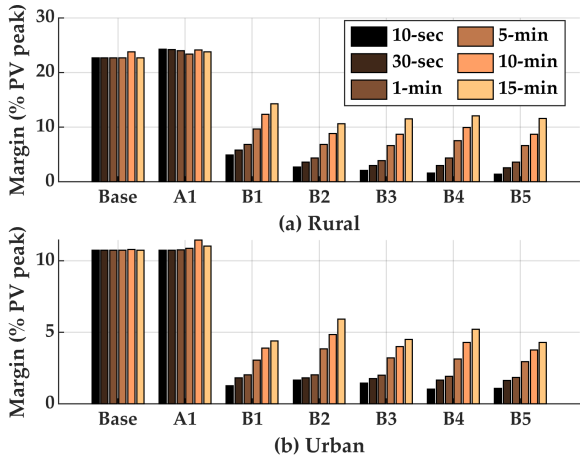

Figure 5.2. PV margin caused by voltage rise at different measurement setups and frequencies in the (a) rural and (b) urban networks.

to the convenient setup B1, optimal setups B2 and B4 have one current meter less, thus yielding a slightly higher PV margin as a result. The results of the 10-minute SE period are higher than the 15-minute SE, which seems counter intuitive at first. However, because the SE takes the latest available pseudo-measured value, the estimation error accumulates in the next 15-minute time step.

Reference Photovoltaic

Figure 5.3 demonstrates that the RPV delivers the downward correction of the voltage estimation. The estimated voltage curve follows the waveform of the actual voltage if it stays below the base case voltage. Moreover, the waveform correction happens at the same frequency as the SE and captures voltage dips that would be otherwise unnoticed by the 15-minute pseudo-measurements. Nevertheless, the upward voltage spikes remain overlooked by the RPV setup. An actual voltage higher than the estimated voltage results in a higher positive estimation error, leading to a higher PV margin. On the other hand, the Mean Absolute Percentage Error (MAPE) for the RPV is lower than the base case. In the case of 10-second SE, MAPE of the RPV case is 0.338%, which is 0.01 percentage point lower than the base case. Even though the setup B1 MAPE is 0.167%, RPV can be misleading in the utilization of the HC.

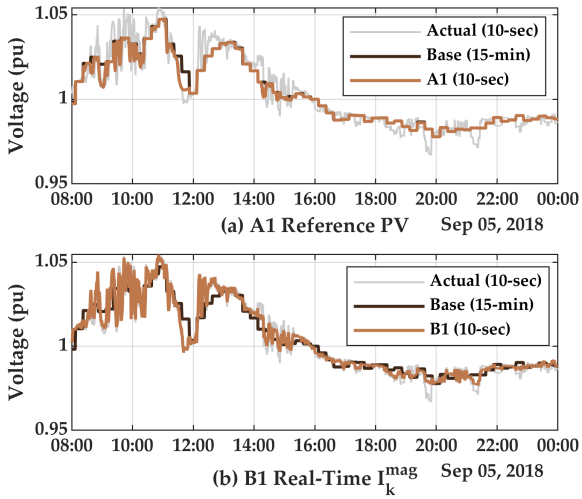

Figure 5.3. Comparison of the phase *a* voltage of the base case with the RPV (A1) and real-time current meter setup (B1) in the rural network.

5.4 Chapter Conclusions

This chapter investigated the practical implications of the hosting capacity. The error of network state estimation was analyzed in terms of PV hosting capacity and was shown to tend to be higher at higher PV penetrations. Low-voltage distribution networks were modeled for balanced and unbalanced PV operations and the estimation error was compared at several metering configurations and SE frequencies. The estimation error was further extended to represent an equivalent PV injected power that has to be decreased to keep the network states within the limits. The proposed PV safety margin was formulated as an optimization problem and shows that the PV hosting capacity in practice is lower than the HC given perfect information of the network states.

The results have shown that the estimation error tends to be larger at higher PV penetration. Also, a mere percentage point of the estimation error can lead to a need for a significant portion of PV power reduction. The PV margin reaches 20% of the PV peak power in the case of pseudo-measurements, while the real-time meters reduce the margin by 2-4 times, thus improving the utilization of the HC. The granularity of real-time measured data has a significant impact on the margin, however is followed by an increased amount of data handling. Finally, a reference PV has been shown as a tool for enhancing pseudo-measurements by nowcasting the generation for nearby PV plants.

6. Discussions

The thesis summarizes research conducted during doctoral studies that explored the PV hosting capacity of low-voltage distribution networks. The thesis tried to find the limits of the hosting capacity and how could the hosting capacity be increased, while also presenting the current situation in the hosting capacity studies, proposing methods to estimate the HC, and which methods could have the highest impact on the HC. During the investigation, the thesis stopped closely at some aspects that, in the author's opinion, were not studied enough. The thesis presented a Monte Carlo simulation for HC evaluation; MIQP formulation of the VU calculation; studied network structure impact on the HC; proposed the slime mold algorithm for network topology generation; and finally discussed how on-site monitoring of networks can impact the HC. However, some questions remained unanswered and could be addressed in future works. These are topics for discussion rather than concrete research problems and are perhaps of more interest to policymakers and could be answered for particular network cases.

For a public discussion, the topic of hosting capacity could be interesting to explore how it could be divided. Considering the HC as a finite resource, can bring some changes in how we perceive it and raise a justified question: how the HC should be divided among the network customers? So far the the division of the HC was not a concern for customers or DSOs. The First Come, First Served principle was historically developed, meaning the customer's PV panel sizes were accepted without considering that the HC is shared between customers of the feeding network (or feeder). A customer who installed a large PV panel first leaves less available HC for his neighbors. That leads to the discussion on how to divide the HC equally between all customers served by a network, LV substation or feeder. With the help of modern simulation tools, PV power injection power can be given to all customers, which would be equal to all customers. It should give equal PV export capacity for all customers while taking into account each customer's unique impedance to the feeding transformer, which causes different voltage rise per unit of injected power. It could be called the right

for power injection. Customers could in fact trade it between each other, comparable to the so-called air rights for high-rise buildings. Finally, from society's point of view, the excess power from the PV generation should be shared and consumed locally. In that case, the highest right for power injection should be given to customers close the large consumption or, simply, close to the feeding transformers [114]. It is of utmost importance to keep the line impedances of customers with PV plants as low as possible to maximize the total injected PV power to the network. In the end, as long as sharing the HC is not yet an alarming issue, the DSOs' and the public's attention will be concerned with other topics.

From a systematic point of view, the hosting capacity can be split into several sub-definitions to cover emerging operational challenges in PV integration. Unlike the methodology presented in this thesis, in reality, the HC is a changing value in time. For example, fast changes in load will change the excess PV generation and cause voltage rise. Accurate network monitoring and state estimation improve situational awareness of voltages and currents in networks and allow estimating the HC in real-time for various DERs control. The HC is a dynamic value and, in addition to real-time, can be forecasted on a short-term basis for a given horizon, for instance, a day ahead HC forecast deducted from weather and load forecasts. For example, the possible regulation of PV feed-in can be regulated by the so-called operating envelopes. These are feed-in constraints that are applied temporarily during high demand or excess generation [115]. Contrary to dynamic HC, this thesis shows yet another type of HC - the worst-case scenario HC calculation. It describes a snapshot of a worst-case time instant over an observed period, for example, a year, and calculates the HC with an optimal power flow method. Such an approach gives an estimate of the HC that is left for future installations, given the load and network parameters remain the same. Moreover, the what-if scenarios can be modeled to evaluate the impact of a possible DER installation, let's say a new PV plant or an EV charging station. Such applications mentioned above can be unified under the term Distributed Energy Resources Management System (DERMS) and have raised significant attention by DSO companies in recent years [116]. Moreover, the HC can be further extended into HC of the installed PV peak power and the feed-in PV power through a point of common coupling. Network reinforcement can increase both the installed and the feed-in powers. However, NWAs can increase the installed PV power by demand response measures of storage, increasing the self-consumption of the PV generation, but keeping the feed-in capacity the same. That has to be taken into account in case of sharing the excess PV power even within a network (or feeder) since the excess power has to pass through the point of common coupling.

Optimal power flow (OPF) algorithms become essential due to the growing need for network operation management. Throughout this study,

several OPF formulations were observed and utilized in some of the works. Most of them that were found in the works were based on the quadratic formulation, which is encapsulated in branch current squared conically constrained by the sum of quadratic active and reactive powers, as in for example [93] and [92]. Unfortunately, such formulations suit minimization problems and were showcased in loss minimization applications. On the other hand, just a few OPF formulations were found to satisfy maximization problems, i.e. hosting capacity studies, for instance, [117]. Reliable distribution network operations with DERs are in great need of linear OPF formulations that can handle voltage rise (in addition to voltage drop), line losses, and active/reactive powers without binary variables. The future of the hosting capacity studies could possibly go along with DER and network operation management.

References

[1] Jaume Duch Guillot. Greenhouse gas emissions by country and sector (infographic). Technical report, European Parliament, 2023.

[2] Roger Fouquet. Path dependence in energy systems and economic development. *Nature Energy*, 1(8):16098, 7 2016.

[3] Eeva-Lotta Apajalahti and Gregor Kungl. Path dependence and path break-out in the electricity sector. *Environmental Innovation and Societal Transitions*, 43:220–236, 6 2022.

[4] Malgorzata Wiatros-Motyka. Global Electricity Review 2023. Technical report, Ember, 2023.

[5] EurObserv'ER. Photovoltaic barometer 2023, 2023.

[6] Secretariat-General European Commission. Communication From the Commission to the European Parliament, the European Council, the Council, the European Economic and Social Committee and the Committee of the Regions Repowereu Plan REPowerEU Plan, 2022.

[7] Henri Hämäläinen and Mervi Suni. Small-scale production of solar electricity grew strongly in 2022, 2023.

[8] Veli-Matti Virtanen and Mervi Suni. Suurten aurinkovoimaloiden tuotantokapasiteetti voi olla jopa 190-kertainen vuoteen 2030 mennessä, 2023.

[9] Yuki Numata, Laurens Speelman, and Marissa Gantman. The Energy Transition Is a Technological Revolution — with a Deadline, 2023.

[10] Abdullah Alshahrani, Siddig Omer, Yuehong Su, Elamin Mohamed, and Saleh Alotaibi. The Technical Challenges Facing the Integration of Small-Scale and Large-scale PV Systems into the Grid: A Critical Review. *Electronics*, 8(12):1443, 12 2019.

[11] Reihaneh Aghamolaei, Mohammad Haris Shamsi, and James O'Donnell. Feasibility analysis of community-based PV systems for residential districts: A comparison of on-site centralized and distributed PV installations. *Renewable Energy*, 157:793–808, 9 2020.

[12] Elering. Elektrituru Käsiraamat. 6.3 Taastuvenergia toomisvõimalused Eestis, 2022.

[13] Svensk Solenergi. Statistik. Installerat antal och effekt, 2023.

[14] Vaasan Sähköverkko. Aurinkopaneelien liitettävyys verkkoon ei ole itsestäänselvyys, 2022.

[15] Elektrilevi. Hiiumaal saavad elektritootjana liituda vaid oma tarbeks tootjad, 2022.

[16] Alfred Jakobsson. Trångt i Dalarnas elnät – kan stoppa den som vill sätta upp solceller, 2023.

[17] Voltage Characteristics of Electricity Supplied by Public Electricity Networks - EN 50160, 2010.

[18] Electric Power Systems And Equipment - Voltage Ratings (60 Hz) - ANSI C84.1, 2020.

[19] Generators Connected to the Low-Voltage Distribution Network - Technical Requirements for the Connection to and Parallel Operation with Low-Voltage Distribution Networks - VDE-AR-N 4105, 2018.

[20] Kshitij Girigoudar and Line A. Roald. On the impact of different voltage unbalance metrics in distribution system optimization. *Electric Power Systems Research*, 189:106656, 12 2020.

[21] Ammar Arshad, Martin Lindner, and Matti Lehtonen. An Analysis of Photo-Voltaic Hosting Capacity in Finnish Low Voltage Distribution Networks. *Energies*, 10(11):1702, 10 2017.

[22] Jouni Räihä. *Heating system decision : a study based on newly built detached houses in Finland*. PhD thesis, University of Oulu, Oulu, 2019.

[23] Jussi Ekström, Matti Koivisto, John Millar, Ilkka Mellin, and Matti Lehtonen. A statistical approach for hourly photovoltaic power generation modeling with generation locations without measured data. *Solar Energy*, 132:173–187, 7 2016.

[24] Christelle Rigollier, Olivier Bauer, and Lucien Wald. On the clear sky model of the ESRA — European Solar Radiation Atlas — with respect to the heliosat method. *Solar Energy*, 68(1):33–48, 1 2000.

[25] Matthew Rylander, Jeff Smith, and Wes Sunderman. Streamlined Method for Determining Distribution System Hosting Capacity. *IEEE Transactions on Industry Applications*, 52(1):105–111, 1 2016.

[26] Farzad Ferdowsi, Shahab Mehraeen, and Gregory B. Upton. Assessing distribution network sensitivity to voltage rise and flicker under high penetration of behind-the-meter solar. *Renewable Energy*, 152:1227–1240, 6 2020.

[27] C.T. Gaunt, E. Namanya, and R. Herman. Voltage modelling of LV feeders with dispersed generation: Limits of penetration of randomly connected photovoltaic generation. *Electric Power Systems Research*, 143:1–6, 2 2017.

[28] Chao Long and Luis F. Ochoa. Voltage Control of PV-Rich LV Networks: OLTC-Fitted Transformer and Capacitor Banks. *IEEE Transactions on Power Systems*, 31(5):4016–4025, 9 2016.

[29] Fei Ding and Barry Mather. On Distributed PV Hosting Capacity Estimation, Sensitivity Study, and Improvement. *IEEE Transactions on Sustainable Energy*, 8(3):1010–1020, 7 2017.

[30] Ricardo Torquato, Diogo Salles, Caio Oriente Pereira, Paulo Cesar Magalhaes Meira, and Walmir Freitas. A Comprehensive Assessment of PV Hosting Capacity on Low-Voltage Distribution Systems. *IEEE Transactions on Power Delivery*, 33(2):1002–1012, 4 2018.

[31] Grabner, Souvent, Suljanović, Košir, and Blažič. Probabilistic Methodology for Calculating PV Hosting Capacity in LV Networks Using Actual Building Roof Data. *Energies*, 12(21):4086, 10 2019.

[32] Iromi Ranaweera, Ole-Morten Midtgård, and Magnus Korpås. Distributed control scheme for residential battery energy storage units coupled with PV systems. *Renewable Energy*, 113:1099–1110, 12 2017.

[33] Daphne Schwanz, Friedemann Möller, Sarah K. Ronnberg, Jan Meyer, and Math H. J. Bollen. Stochastic Assessment of Voltage Unbalance Due to Single-Phase-Connected Solar Power. *IEEE Transactions on Power Delivery*, 32(2):852–861, 4 2017.

[34] Elson N.M. Silva, Anselmo B. Rodrigues, and Maria da Guia da Silva. Stochastic assessment of the impact of photovoltaic distributed generation on the power quality indices of distribution networks. *Electric Power Systems Research*, 135:59–67, 6 2016.

[35] Z. Liu and J. V. Milanovic. Probabilistic Estimation of Voltage Unbalance in MV Distribution Networks With Unbalanced Load. *IEEE Transactions on Power Delivery*, 30(2):693–703, 4 2015.

[36] F.J. Ruiz-Rodriguez, J.C. Hernández, and F. Jurado. Voltage unbalance assessment in secondary radial distribution networks with single-phase photovoltaic systems. *International Journal of Electrical Power & Energy Systems*, 64:646–654, 1 2015.

[37] Anamika Dubey, Surya Santoso, and Arindam Maitra. Understanding photovoltaic hosting capacity of distribution circuits. In *2015 IEEE Power & Energy Society General Meeting*, pages 1–5. IEEE, 7 2015.

[38] Ali Kharrazi, Victor Sreeram, and Yateendra Mishra. Assessment of voltage unbalance due to single phase rooftop photovoltaic panels in residential low voltage distribution network: A study on a real LV network in Western Australia. In *2017 Australasian Universities Power Engineering Conference (AUPEC)*, pages 1–6. IEEE, 11 2017.

[39] Mahyar Abasi, S. Ghodratollah Seifossadat, Morteza Razaz, and S. Sajad Moosapour. Determining the contribution of different effective factors to individual voltage unbalance emission in n-bus radial power systems. *International Journal of Electrical Power & Energy Systems*, 94:393–404, 1 2018.

[40] Yuanyuan Sun, Peixin Li, Shurong Li, and Linghan Zhang. Contribution Determination for Multiple Unbalanced Sources at the Point of Common Coupling. *Energies*, 10(2):171, 2 2017.

[41] Hassan Feshki Farahani. Improving voltage unbalance of low-voltage distribution networks using plug-in electric vehicles. *Journal of Cleaner Production*, 148:336–346, 4 2017.

[42] Jian Xu, Jing Wang, Siyang Liao, Yuanzhang Sun, Deping Ke, Xiong Li, Ji Liu, Yibo Jiang, Congying Wei, and Bowen Tang. Stochastic multi-objective optimization of photovoltaics integrated three-phase distribution network based on dynamic scenarios. *Applied Energy*, 231:985–996, 12 2018.

[43] Bharath Rao, Friederich Kupzog, and Martin Kozek. Three-Phase Unbalanced Optimal Power Flow Using Holomorphic Embedding Load Flow Method. *Sustainability*, 11(6):1774, 3 2019.

[44] Md. Rabiul Islam, Haiyan Lu, Jahangir Hossain, Md. Rabiul Islam, and Li Li. Multiobjective Optimization Technique for Mitigating Unbalance and Improving Voltage Considering Higher Penetration of Electric Vehicles and Distributed Generation. *IEEE Systems Journal*, 14(3):3676–3686, 9 2020.

[45] Francisco Coelho, Wesley Peres, Ivo Silva Junior, and Bruno Dias. An Empirical Continuous Metaheuristic for Multiple Distributed Generation Scheduling Considering Energy Loss Minimization, Voltage and Unbalance Regulatory Limit. *IET Generation, Transmission & Distribution*, 5 2020.

[46] Jeremy Donald Watson, Neville R. Watson, and Ioannis Lestas. Optimized Dispatch of Energy Storage Systems in Unbalanced Distribution Networks. *IEEE Transactions on Sustainable Energy*, 9(2):639–650, 4 2018.

[47] Luna Forte de Oliveira, Diogo Jose, Paulo Renato da Costa Mendes, and Julio Elias Normey-Rico. A Convex Optimal Voltage Unbalance Compensator for Hybrid AC/DC Microgrids. In *2019 IEEE PES Innovative Smart Grid Technologies Conference - Latin America (ISGT Latin America)*, pages 1–6. IEEE, 9 2019.

[48] Mojtaba Sepehry, Mohammad Heidari Kapourchali, Visvakumar Aravinthan, and Ward Jewell. Robust Day-Ahead Operation Planning of Unbalanced Microgrids. *IEEE Transactions on Industrial Informatics*, 15(8):4545–4557, 8 2019.

[49] Peng Li, Haoran Ji, Chengshan Wang, Jinli Zhao, Guanyu Song, Fei Ding, and Jianzhong Wu. Optimal Operation of Soft Open Points in Active Distribution Networks Under Three-Phase Unbalanced Conditions. *IEEE Transactions on Smart Grid*, 10(1):380–391, 1 2019.

[50] Thorsten Gross, Sven Reese, Benjamin Petters, Marco Cupelli, Dominik Mildt, and Antonello Monti. A Novel Approach to DG Curtailment in Rural Distribution Networks – A Case Study of the Avacon Grid as Part of the InterFlex Field Trial. In *2018 IEEE 16th International Conference on Industrial Informatics (INDIN)*, pages 667–672. IEEE, 7 2018.

[51] Till Luhmann, Enno Wieben, Riccardo Treydel, Michael Stadler, and Thomas Kumm. An Approach for Cost-Efficient Grid Integration of Distributed Renewable Energy Sources. *Engineering*, 1(4):447–452, 12 2015.

[52] Daesoo Kim, Hoejun Kim, and Dongjun Won. Operation Strategy of Shared ESS Based on Power Sensitivity Analysis to Minimize PV Curtailment and Maximize Profit. *IEEE Access*, 8:197097–197110, 2020.

[53] Mingtao Ma, Huijun Huang, Xiaoling Song, Feniosky Peña-Mora, Zhe Zhang, and Jie Chen. Optimal sizing and operations of shared energy storage systems in distribution networks: A bi-level programming approach. *Applied Energy*, 307:118170, 2 2022.

[54] Roman Bolgaryn, Zhenqi Wang, Alexander Scheidler, and Martin Braun. Active Power Curtailment in Power System Planning. *IEEE Open Access Journal of Power and Energy*, 8:399–408, 2021.

[55] Henrik Klinge Jacobsen and Sascha Thorsten Schröder. Curtailment of renewable generation: Economic optimality and incentives. *Energy Policy*, 49:663–675, 10 2012.

[56] B. Bletterie, S. Kadam, and J. Le Baut. Increased hosting capacity by means of active power curtailment. In *CIRED Workshop 2016*, pages 194 (4 .)–194 (4 .). Institution of Engineering and Technology, 2016.

[57] Merlinda Andoni, Valentin Robu, Wolf-Gerrit Früh, and David Flynn. Game-theoretic modeling of curtailment rules and network investments with distributed generation. *Applied Energy*, 201:174–187, 9 2017.

[58] Energy Authority. Regulation Methods in the Fourth Regulatory Period of 1 January 2016–31 December 2019 and the Fifth Regulatory Period of 1 January 2020–31 December 2023; Appendix 2. Technical report, Energy Authority, Helsinki, Finland, 2015.

[59] Prysmian Group. AXMK-PLUS 4-johtiminen: Alumiinijohtiminen PEX-eristeinen halogeeniton 1 kV voimakaapeli.

[60] ABB. Liquid-filled distribution transformers.

[61] Jussi Vimpari and Seppo Junnila. Estimating the diffusion of rooftop PVs: A real estate economics perspective. *Energy*, 172:1087–1097, 4 2019.

[62] J.M. Nahman and D.M. Peric. Optimal Planning of Radial Distribution Networks by Simulated Annealing Technique. *IEEE Transactions on Power Systems*, 23(2):790–795, 5 2008.

[63] Sachin Singh, T. Ghose, and S. K. Goswami. Optimal Feeder Routing Based on the Bacterial Foraging Technique. *IEEE Transactions on Power Delivery*, 27(1):70–78, 1 2012.

[64] Jun Shu, Lei Wu, Lizi Zhang, and Bing Han. Spatial Power Network Expansion Planning Considering Generation Expansion. *IEEE Transactions on Power Systems*, 30(4):1815–1824, 7 2015.

[65] K. Nara. A new algorithm for distribution feeder expansion planning for urban area. In *APSCOM-97. International Conference on Advances in Power System Control, Operation and Management*, volume 1997, pages 192–197. IEE, 1997.

[66] Pouya Salyani, Javad Salehi, and Farhad Samadi Gazijahani. Chance constrained simultaneous optimization of substations, feeders, renewable and non-renewable distributed generations in distribution network. *Electric Power Systems Research*, 158:56–69, 5 2018.

[67] Mohamed Yosef, M.M. Sayed, and Hosam K.M. Youssef. Allocation and sizing of distribution transformers and feeders for optimal planning of MV/LV distribution networks using optimal integrated biogeography based optimization method. *Electric Power Systems Research*, 128:100–112, 11 2015.

[68] J. C. Moreira, E. Miguez, C. Vilacha, and Antonio F. Otero. Large-Scale Network Layout Optimization for Radial Distribution Networks by Parallel Computing: Implementation and Numerical Results. *IEEE Transactions on Power Delivery*, 27(3):1468–1476, 7 2012.

[69] S. Najafi Ravadanfegh and R. Gholizadeh Roshanagh. On optimal multistage electric power distribution networks expansion planning. *International Journal of Electrical Power & Energy Systems*, 54:487–497, 1 2014.

[70] Shahram Mojtahedzadeh, Sajad Najafi Ravadanegh, and Mahmoud-Reza Haghifam. Optimal multiple microgrids based forming of greenfield distribution network under uncertainty. *IET Renewable Power Generation*, 11(7):1059–1068, 6 2017.

[71] Mahmood Kalantari Khandani and Alireza Askarzadeh. Optimal MV/LV transformer allocation in distribution network for power losses reduction and cost minimization: A new multi-objective framework. *International Transactions on Electrical Energy Systems*, 30(6), 6 2020.

[72] Y.-Y. Hong and S.-Y. Ho. Determination of Network Configuration Considering Multiobjective in Distribution Systems Using Genetic Algorithms. *IEEE Transactions on Power Systems*, 20(2):1062–1069, 5 2005.

[73] Wenjun Zhang, Haozhong Cheng, Saiyi Wang, Yinong Li, and Jianmin Wang. Distribution network planning based on tree structure encoding partheno-genetic algorithm. In *2008 Third International Conference on Electric Utility Deregulation and Restructuring and Power Technologies*, pages 1399–1406. IEEE, 4 2008.

[74] S. Najafi, S.H. Hosseinian, M. Abedi, A. Vahidnia, and S. Abachezadeh. A Framework for Optimal Planning in Large Distribution Networks. *IEEE Transactions on Power Systems*, 24(2):1019–1028, 5 2009.

[75] Luis Gonzalez-Sotres, Carlos Mateo Domingo, Alvaro Sanchez-Miralles, and Manuel Alvar Miro. Large-Scale MV/LV Transformer Substation Planning Considering Network Costs and Flexible Area Decomposition. *IEEE Transactions on Power Delivery*, 28(4):2245–2253, 10 2013.

[76] Reza Gholizadeh-Roshanagh, Sajad Najafi-Ravadanegh, and Seyed Hossein Hosseinian. A Framework for Optimal Coordinated Primary-Secondary Planning of Distribution Systems Considering MV Distributed Generation. *IEEE Transactions on Smart Grid*, 9(2):1408–1415, 3 2018.

[77] David Ciechanowicz, Dominik Pelzer, Benedikt Bartenschlager, and Alois Knoll. A Modular Power System Planning and Power Flow Simulation Framework for Generating and Evaluating Power Network Models. *IEEE Transactions on Power Systems*, 32(3):2214–2224, 5 2017.

[78] James R. E. Fletcher, Tyrone Fernando, Herbert Ho-Ching Iu, Mark Reynolds, and Shervin Fani. Spatial Optimization for the Planning of Sparse Power Distribution Networks. *IEEE Transactions on Power Systems*, 33(6):6686–6695, 11 2018.

[79] Verner Püvi and Matti Lehtonen. Evaluating distribution network optimal structure with respect to solar hosting capacity. *Electric Power Systems Research*, 216:109019, 3 2023.

[80] Vincenzo Bonifaci, Kurt Mehlhorn, and Girish Varma. Physarum can compute shortest paths. *Journal of Theoretical Biology*, 309:121–133, 9 2012.

[81] Atsushi Tero, Ryo Kobayashi, and Toshiyuki Nakagaki. A mathematical model for adaptive transport network in path finding by true slime mold. *Journal of Theoretical Biology*, 244(4):553–564, 2 2007.

[82] Liang Liu, Yuning Song, Haiyang Zhang, Huadong Ma, and Athanasios V. Vasilakos. Physarum Optimization: A Biology-Inspired Algorithm for the Steiner Tree Problem in Networks. *IEEE Transactions on Computers*, 64(3):818–831, 3 2015.

[83] Yahui Sun and Saman Halgamuge. Fast algorithms inspired by Physarum polycephalum for node weighted steiner tree problem with multiple terminals. In *2016 IEEE Congress on Evolutionary Computation (CEC)*, pages 3254–3260. IEEE, 7 2016.

[84] A. Tero, S. Takagi, T. Saigusa, K. Ito, D. P. Bebber, M. D. Fricker, K. Yumiki, R. Kobayashi, and T. Nakagaki. Rules for Biologically Inspired Adaptive Network Design. *Science*, 327(5964):439–442, 1 2010.

[85] Shin Watanabe, Atsushi Tero, Atsuko Takamatsu, and Toshiyuki Nakagaki. Traffic optimization in railroad networks using an algorithm mimicking an amoeba-like organism, Physarum plasmodium. *Biosystems*, 105(3):225–232, 9 2011.

[86] Michail-Antisthenis I. Tsompanas, Georgios C. Sirakoulis, and Andrew I. Adamatzky. Evolving Transport Networks With Cellular Automata Models Inspired by Slime Mould. *IEEE Transactions on Cybernetics*, 45(9):1887–1899, 9 2015.

[87] Xiaoge Zhang, Andrew Adamatzky, Xin-She Yang, Hai Yang, Sankaran Mahadevan, and Yong Deng. A Physarum-inspired approach to supply chain network design. *Science China Information Sciences*, 59(5):052203, 5 2016.

[88] Chao Gao, Shi Chen, Xianghua Li, Jiajin Huang, and Zili Zhang. A Physarum-inspired optimization algorithm for load-shedding problem. *Applied Soft Computing*, 61:239–255, 12 2017.

[89] Shin Watanabe and Atsuko Takamatsu. Transportation Network with Fluctuating Input/Output Designed by the Bio-Inspired Physarum Algorithm. *PLoS ONE*, 9(2):e89231, 2 2014.

[90] Hiroshi Katada, Taku Yamazaki, and Takumi Miyoshi. Performance Analysis of Physarum-based Multi-hop Routing with Load Balancing. In *2019 12th IFIP Wireless and Mobile Networking Conference (WMNC)*, pages 118–125. IEEE, 9 2019.

[91] Robert John Millar, Eero Saarijärvi, and Matti Lehtonen. An Improved Initial Network for Distribution Network Planning Algorithms. *International Review of Electrical Engineering (IREE)*, 9(3):538, 6 2014.

[92] Mohammad Reza Dorostkar-Ghamsari, Mahmud Fotuhi-Firuzabad, Matti Lehtonen, and Amir Safdarian. Value of Distribution Network Reconfiguration in Presence of Renewable Energy Resources. *IEEE Transactions on Power Systems*, 31(3):1879–1888, 5 2016.

[93] Joshua A. Taylor and Franz S. Hover. Convex Models of Distribution System Reconfiguration. *IEEE Transactions on Power Systems*, 27(3):1407–1413, 8 2012.

[94] N. Efkarpidis, T. De Rybel, and J. Driesen. Optimization control scheme utilizing small-scale distributed generators and OLTC distribution transformers. *Sustainable Energy, Grids and Networks*, 8:74–84, 12 2016.

[95] Arslan Ahmad Bashir, Mahdi Pourakbari-Kasmaei, Javier Contreras, and Matti Lehtonen. A novel energy scheduling framework for reliable and economic operation of islanded and grid-connected microgrids. *Electric Power Systems Research*, 171:85–96, 6 2019.

[96] Tuukka Sandell. *Sähkön hajautetun pientuotannon kehitys jakeluverkoissa ja vaikutukset verkon käyttöön*. PhD thesis, Aalto University, 2021.

[97] Grazia Barchi and David Macii. A photovoltaics-aided interlaced extended Kalman filter for distribution systems state estimation. *Sustainable Energy, Grids and Networks*, 26:100438, 6 2021.

[98] Gang Cheng, Shaojian Song, Yuzhang Lin, Qingbao Huang, Xiaofeng Lin, and Fei Wang. Enhanced state estimation and bad data identification in active power distribution networks using photovoltaic power forecasting. *Electric Power Systems Research*, 177:105974, 12 2019.

[99] A.K. Al-Othman and M.R. Irving. Analysis of confidence bounds in power system state estimation with uncertainty in both measurements and parameters. *Electric Power Systems Research*, 76(12):1011–1018, 8 2006.

[100] Nils Müller, Samuel Chevalier, Carsten Heinrich, Kai Heussen, and Charalampos Ziras. Uncertainty quantification in LV state estimation under high shares of flexible resources. *Electric Power Systems Research*, 212:108479, 11 2022.

[101] Wele Gedara Chaminda Bandara, Dilini Almeida, Roshan Indika Godaliyadda, Mervyn Parakrama Ekanayake, and Janaka Ekanayake. A complete state estimation algorithm for a three-phase four-wire low voltage distribution system with high penetration of solar PV. *International Journal of Electrical Power & Energy Systems*, 124:106332, 1 2021.

[102] Annika Bruggemann, Christian Rehtanz, and Theresa Noll. Analysis of State Uncertainty for Distribution System State Estimation. In *2019 IEEE Milan PowerTech*, pages 1–6. IEEE, 6 2019.

[103] Marta Vanin, Tom Van Acker, Reinhilde D'hulst, and Dirk Van Hertem. Exact Modeling of Non-Gaussian Measurement Uncertainty in Distribution System State Estimation. *IEEE Transactions on Instrumentation and Measurement*, 72:1–11, 2023.

[104] Niels Blaauwbroek, Dirk Kuiken, Phuong Nguyen, Hans Vedder, Martha Roggenkamp, and Han Slootweg. Distribution network monitoring: Interaction between EU legal conditions and state estimation accuracy. *Energy Policy*, 115:78–87, 4 2018.

[105] Mojtaba Ajoudani, Abdolreza Shiekholeslami, and Alireza Zakariazadeh. Improving state estimation accuracy in active distribution networks by coordinating real-time and pseudo-measurements considering load uncertainty. *IET Generation, Transmission & Distribution*, 16(8):1620–1638, 4 2022.

[106] Ali Abur and Antonio Gómez Expósito. *Power System State Estimation*. CRC Press, 3 2004.

[107] Markos Asprou and Elias Kyriakides. Enhancement of hybrid state estimation using pseudo flow measurements. In *2011 IEEE Power and Energy Society General Meeting*, pages 1–7. IEEE, 7 2011.

[108] George N. Korres and Nikolaos M. Manousakis. A state estimator including conventional and synchronized phasor measurements. *Computers & Electrical Engineering*, 38(2):294–305, 3 2012.

[109] Xiaoshuang Chen, Jin Lin, Can Wan, Yonghua Song, Shi You, Yi Zong, Wanfang Guo, and Yuanxi Li. Optimal Meter Placement for Distribution Network State Estimation: A Circuit Representation Based MILP Approach. *IEEE Transactions on Power Systems*, 31(6):4357–4370, 11 2016.

[110] Diogo M.V.P. Ferreira, Pedro M.S. Carvalho, and Luís A.F.M. Ferreira. Optimal Meter Placement in Low Observability Distribution Networks with DER. *Electric Power Systems Research*, 189:106707, 12 2020.

[111] Zhiyi Zhao, Ying Xue, Zhaoxi Liu, Weiye Zheng, Shuyin Duan, and Lei Yu. A novel estimation method for maximum PV hosting capacity in radial distribution networks using bus voltage and electrical distance. *Electric Power Systems Research*, 224:109791, 11 2023.

[112] Jamie M. Bright, Sven Killinger, David Lingfors, and Nicholas A. Engerer. Improved satellite-derived PV power nowcasting using real-time power data from reference PV systems. *Solar Energy*, 168:118–139, 7 2018.

[113] Bishnu Nepal, Motoi Yamaha, Aya Yokoe, and Toshiya Yamaji. Electricity load forecasting using clustering and ARIMA model for energy management in buildings. *Japan Architectural Review*, 3(1):62–76, 1 2020.

[114] Alexandre Lucas. Single-Phase PV Power Injection Limit due to Voltage Unbalances Applied to an Urban Reference Network Using Real-Time Simulation. *Applied Sciences*, 8(8):1333, 8 2018.

[115] Kyriacos Petrou, Michael Z. Liu, Andreas T. Procopiou, Luis F. Ochoa, John Theunissen, and Justin Harding. Operating Envelopes for Prosumers in LV Networks: A Weighted Proportional Fairness Approach. In *2020 IEEE PES Innovative Smart Grid Technologies Europe (ISGT-Europe)*, pages 579–583. IEEE, 10 2020.

[116] Juan Castaneda and Andrew Ioan. Electric Access System Enhancement (EASE): Assessment of a Distributed Energy Resource Management System for Enabling Dynamic Hosting Capacity. Technical report, Golden Field Office, Golden, CO (United States), 4 2022.

[117] Mansoor Alturki, Amin Khodaei, Aleksi Paaso, and Shay Bahramirad. Optimization-based distribution grid hosting capacity calculations. *Applied Energy*, 219:350–360, 6 2018.

Aalto-DT 129/2024

ISBN 978-952-64-1884-1 (printed)
ISBN 978-952-64-1885-8 (pdf)
ISSN 1799-4934 (printed)
ISSN 1799-4942 (pdf)

Aalto University
School of Electrical Engineering
Department of Electrical Engineering and Automation
www.aalto.fi

BUSINESS + ECONOMY

ART + DESIGN + ARCHITECTURE

SCIENCE + TECHNOLOGY

CROSSOVER

DOCTORAL THESES